Reconstituting Placenta–Embryo Crosstalk in a Microfluidic Chip for Human-Relevant Developmental Toxicity Studies

Tina Buerki-Thurnherr

tina.buerki@empa.ch

Swiss Federal Laboratories for Materials Science and Technology https://orcid.org/0000-0003-3723-6562

Manon Murdeu

Swiss Federal Laboratories for Materials Science and Technology

Isabel Wegner

Swiss Federal Institute of Technology Zurich

Xialein Lin

Swiss Federal Institute of Technology Zurich

Jacob Folz

Swiss Federal Institute of Technology Zurich

Paula Navascués

Swiss Federal Laboratories for Materials Science and Technology https://orcid.org/0000-0002-2762-6527

Andreas Hierlemann

ETH Zurich https://orcid.org/0000-0002-3838-2468

Julia A. Boos

ETH Zurich

Vera Kissling

Swiss Federal Laboratories for Materials Science and Technology https://orcid.org/0000-0002-4524-9905

Article

Keywords:

Posted Date: August 4th, 2026

DOI: https://doi.org/10.21203/rs.3.rs-8945339/v1

Additional Declarations: There is **NO** Competing Interest.

Reconstituting Placenta-Embryo Crosstalk in a Microfluidic Chip for Human-Relevant Developmental Toxicity Studies

Manon Murdeu[1,2], Isabel Wegner[2], Xiaolei Lin[2], Vera M. Kissling[1], Jacob Folz[3], Paula Navascués[4], Andreas Hierlemann[2], Julia A. Boos[2,5,6 ¥], Tina Buerki-Thurnherr[1 ¥]

[1]Laboratory for Nanomaterials in Health, Swiss Federal Laboratories for Materials Science and Technology (Empa), 9014 St. Gallen, Switzerland
[2]Bioengineering Laboratory, Department of Biosystems Science and Engineering, ETH Zürich, 4056 Basel, Switzerland
[3]Department of Health Sciences and Technology, ETH Zürich, 8092 Zürich, Switzerland
[4]Laboratory for Advanced Fibers, Swiss Federal Laboratories for Materials Science and Technology (Empa), 9014 St. Gallen, Switzerland
[5]SCAHT - Swiss Centre for Applied Human Toxicology, 4055 Basel, Switzerland
[6]Department of Pharmaceutical Sciences, University of Basel, 4001 Basel, Switzerland

¥ Shared last author

Tina Buerki-Thurnherr
E-mail: tina.buerki@empa.ch
Orcid ID: 0000-0003-3723-6562

Julia Boos
E-mail: julia.boos@unibas.ch
Orcid ID: 0000-0001-9490-9810

Abstract

Developmental toxicity assessment currently relies predominantly on in vivo animal studies that provide limited mechanistic insights into human-relevant effects of drugs, nanoparticles (NPs), or environmental pollutants during pregnancy. To bridge this gap, we developed an innovative human-based co-culture platform on a microfluidic chip that integrates a placental barrier model with a human induced pluripotent stem cell (hiPSC)-derived embryoid body (EB) to model early embryonic development. The placental model consists of primary cytotrophoblast (CTB) cells from human term placenta and human placental vascular endothelial cells (HPVECs). CTBs formed a spontaneous syncytialized trophoblast layer with preserved endocrine function and predictable transport of drugs and NPs, while EBs maintained germ-layer differentiation capacity during co-culturing. Exposure to the known teratogen valproic acid disrupted neuroectodermal features in EBs only in the presence of the placental barrier, while the placenta prevented the accumulation of all-trans retinoic acid in the embryonic compartment, demonstrating that placental transport, metabolism, and signalling actively modulate developmental toxicity outcomes. Overall, our platform reproduces key features of the dynamic placenta-embryo interplay and provides a human-relevant in vitro system for mechanistic studies of placental contributions to developmental toxicity.

MAIN

Increasing industrialization and human activity have raised exposure to chemicals, nanoparticles (NPs), and environmental pollutants, all of which bear significant health risks, particularly during sensitive life stages, such as pregnancy.[1–3] At the same time, medication intake by pregnant women has steadily increased in the last decades, while robust scientific evidence on the safety, efficacy, and appropriate dosing of pharmacological therapies in this vulnerable population remains limited.[4–8] Investigating and addressing these health risks is challenged by the lack of predictive, human-relevant models that can reproduce maternal-foetal transport and elucidate how maternal exposures translate into adverse developmental outcomes.

In recent years, substantial progress has been made in establishing in vitro assays for evaluating developmental toxicity.[9] This progress has resulted in the development of both, ECVAM-validated approaches[10,11] and commercially available platforms, that primarily rely on differentiation-based readouts and cytotoxicity metrics.[12] More recently, human induced pluripotent stem cell (hiPSC)-derived embryoid bodies (EBs), which differentiate into the three germ layers, have emerged as promising human-relevant tool for in vitro teratogenicity assessment.[13,14] However, the available models generally rely on direct exposure of embryonic systems to test compounds and do not capture the critical role of the placenta in modulating embryo-foetal exposure and toxicity mechanisms.

The human placenta, a transient, yet highly specialized organ, interconnects maternal and foetal circulation, mediates transport and metabolic exchange of molecules and compounds, endocrine signalling, as well as immune modulation, and provides protection for the developing embryo throughout gestation.[15] Its functional units, the chorionic villi, feature a highly vascularized architecture extending from the chorionic plate, facing the foetus, to the maternal decidua. Within each villus, foetal endothelial cells line the vascular network in a stromal core, while mononucleated cytotrophoblast (CTB) cells progressively fuse to form the outer, multinucleated syncytiotrophoblast (STB) layer in direct contact with maternal blood.[16] Together, trophoblast layers and foetal endothelium constitute the placental barrier that governs molecular transport and foetal exposure.

To mimic this interface in vitro and assess compound transport, various placental models have been developed, primarily using membrane-supported mono- or co-cultures of trophoblast cells, derived from primary tissue[17,18] or cell lines, such as BeWo b30,[19,20] combined with endothelial cells.[21] Placental models on microfluidic platforms have incorporated flow to better approximate physiological transport dynamics and, in some cases, extracellular matrix-mimicking materials,

such as hydrogels.[22] While these systems enable quantitative studies of barrier integrity, transport kinetics, and mechanobiology, they do not include embryonic tissue, which precludes a direct assessment of foetal responses to placental perturbation.

We previously demonstrated the feasibility of coupling placental transport with downstream developmental readouts using a prototype microphysiological system that integrates a cell line-derived trophoblast barrier with murine EBs.[23] Here, we advance this concept by engineering a fully human-based co-culture platform that combines a functional placental barrier, composed of primary trophoblast cells and placental vascular endothelial cells (HPVECs), with a human iPSC-derived embryo model in a microfluidic system. The placental and embryonic tissues are cultured in close proximity, enabling continuous inter-tissue communication supported by gravity-driven flow. Using valproic acid (VPA) and all-trans retinoic acid (RA) as reference teratogens,[9] we show that VPA-induced disruption of neuroectodermal features occurs only in the presence of the placental barrier, whereas RA exposure is attenuated by the placental metabolism resulting in no notable toxicity for the EBs. These results evidence the placental barrier's active role in regulating embryonic/foetal exposure and underscores the importance of incorporating placental function in developmental toxicity assessment.

RESULTS

Modelling the placenta-embryonic interface

To guide the design of a human relevant maternal-embryonic interface on a chip, we considered the in vivo-architecture of the human placenta as a biological reference (Fig. 1a). In vivo, the placental villi are highly vascularized tree-like structures bathing in maternal blood. Foetal blood vessels are enclosed within a stromal core containing fibroblasts and foetal macrophages (Hofbauer cells). In contact with the basal lamina, rich in collagen IV, mononuclear cytotrophoblast (CTB) cells fuse to form the outer multinucleated syncytiotrophoblast (STB), which is in direct contact with the maternal blood. Together, the STB, CTBs and foetal endothelium constitute the placental barrier at the maternal-embryonic interface.

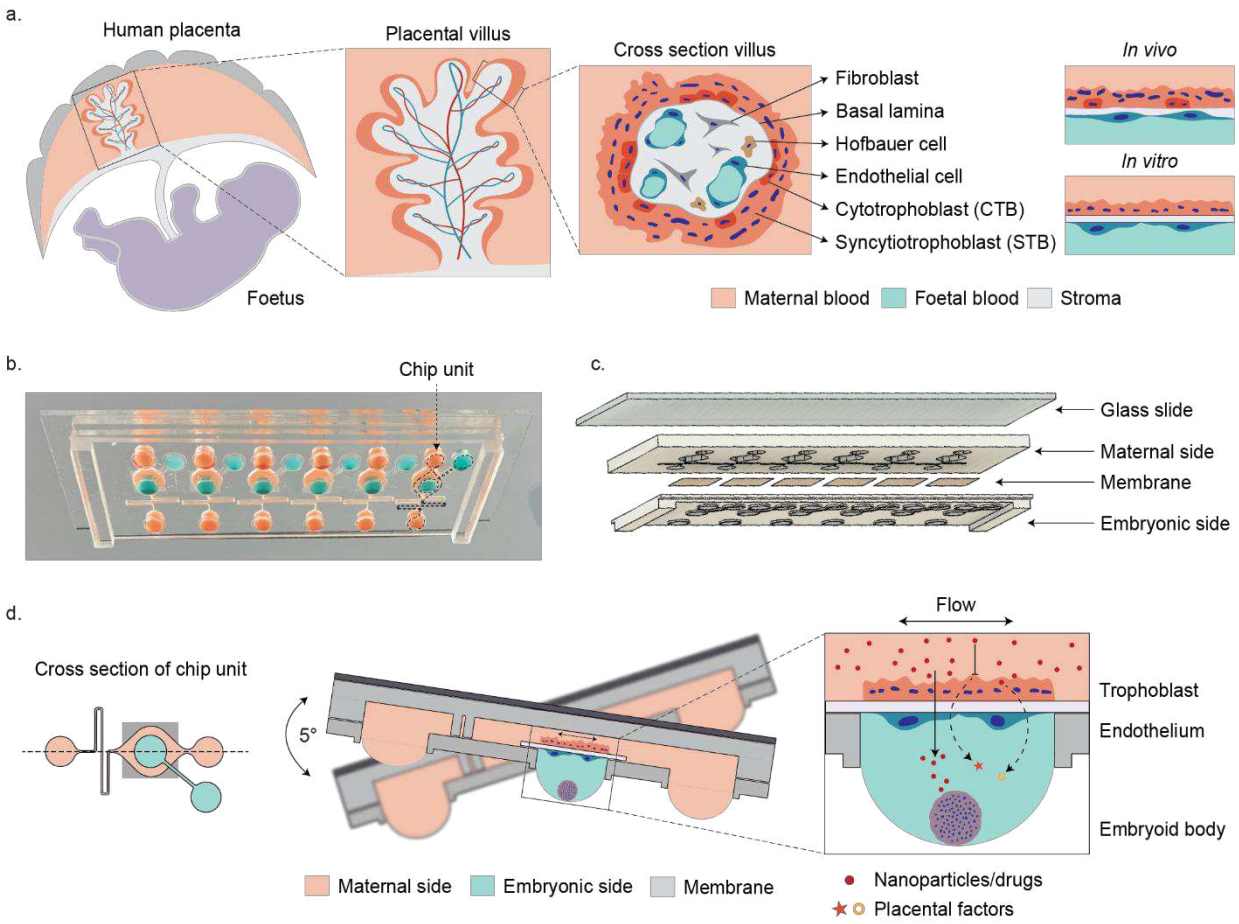

Fig. 1: In vivo schematic of the human placental structure and cellular composition and in vitro microfluidic chip model. a, The placenta comprises highly vascularized chorionic villi, the cross-section of which reveals foetal capillaries within a stromal core adjacent to trophoblast layers, where cytotrophoblasts fuse to form the outer syncytiotrophoblast in direct contact with maternal blood. **b,** The microfluidic device comprises six independent units, each featuring a maternal cell culture area (pink) and an embryonic compartment (blue). **c,** The microfluidic platform includes two PDMS layers, representing the maternal and embryonic sides, separated by a porous membrane and stabilized on a glass slide. **d,** The cross-section of the microfluidic unit reveals the in vitro biological model, where trophoblast cells and endothelial cells are cultured on opposite sides of a porous membrane to mimic the placental barrier in proximity to a hiPSCs-derived EB as a model of early embryonic development.

To recapitulate this interface in vitro, we developed a microfluidic hanging-drop platform that enables the direct co-culturing of a placental barrier and an embryoid body (EB), modelling early embryonic development (Fig. 1b). The microfluidic chip consists of two poly(dimethylsiloxane) (PDMS) parts separated by a semipermeable polyethylene terephthalate (PET) membrane with 1 µm pore size (Fig. 1c). For structural stability, the assembled device is bonded to a microscopy glass slide. The membrane forms a physical interface between two vertically aligned fluidic

compartments, referred to as the maternal and embryonic compartments. Each chip contains six independent fluidic units that can be operated in parallel on a single platform.

A cross-section of one unit is shown in Fig. 1d. A central culture chamber hosts the placental barrier, with primary human placenta-derived CTBs seeded on the maternal side and HPVECs on the embryonic side of the membrane. The maternal compartment is accessible through two lateral hanging drops that allow medium exchange and nutrient supply. A meander-shaped microchannel connects one of the drops to the culture chamber, introducing defined flow resistance and enabling modulation of the perfusion rate across the barrier. The embryonic compartment consists of a hanging drop positioned directly beneath the membrane, where the EB is cultured in immediate proximity to the placental barrier. This drop is connected to a secondary hanging drop via a microfluidic channel that provides an access point for medium exchange, enables the induction of a gentle flow, and increases the available culture volume (Supplementary Fig 1 a, b and c).

To minimize absorption and adsorption of small molecules and NPs, the PDMS surface facing the culture media was coated using a plasma-deposited organosilicon thin film with SiO:CH chemistry. The film thickness, determined by profilometry, was 265 ± 5 nm. Additional platform features and thin-film characterization are provided in Supplementary Fig. 1.

Bidirectional tilting of the device by ±5° induces gravity-driven flow, enabling the exchange of nutrients, signalling molecules and other secretory factors between the placenta and EB. Consequently, the platform enables not only transport studies to investigate direct embryotoxic effects of compounds crossing the placental barrier, but also the study of indirect developmental toxicity resulting from perturbations in the placental tissue that alter signalling pathways and factors that are important for embryo development.

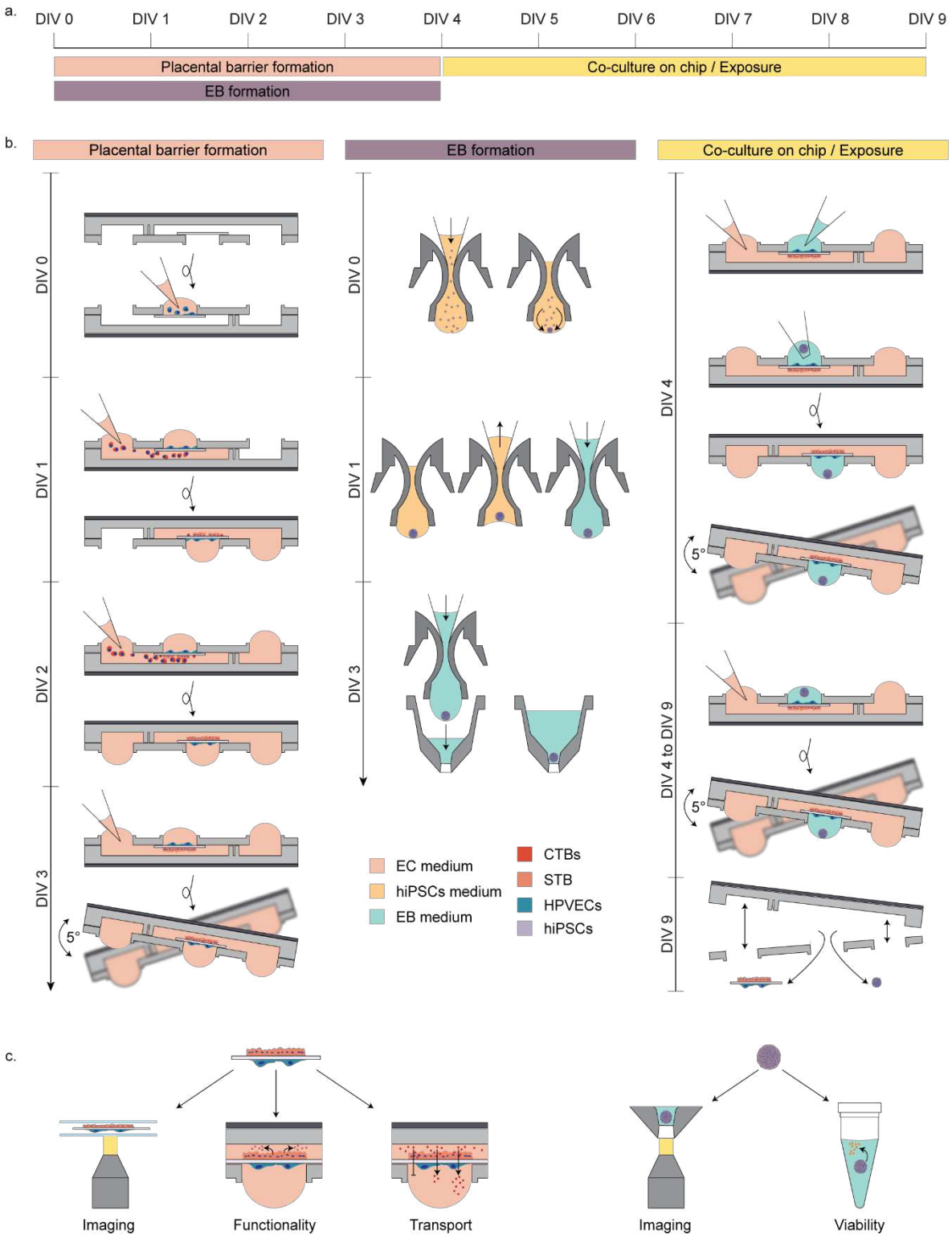

Fig. 2: Timeline and experimental workflow of the co-culture model. a-b, Experimental timeline and schematic representation of the workflow: From DIV0 to DIV4, the placental barrier was established on chip, while EBs were formed on Akura™ hanging drop plates. On DIV4, EBs were transferred to the chip for co-culture or exposure, which

continued until DIV9. **c,** Readouts and endpoints of the co-culture. Placental barrier was analysed for morphology (confocal imaging, TEM, SEM), functionality (hCG secretion) and transport characteristics (permeability markers, drugs, NPs). EB endpoints included morphology and differentiation (light microscopy, confocal imaging) and viability (intracellular ATP). Abbreviation: Day in vitro (DIV).

To recreate the maternal-embryonic axis and enable toxicity assessment, we established the experimental workflow shown in Fig 2. During the first four days in vitro (DIV0-4), the placental barrier was established on-chip, while EBs were formed and differentiated in parallel in hanging-drop well plate cultures. On DIV4, EBs were transferred to the chip to initiate co-culturing, which was continued for five additional days to perform the exposure assays (Fig. 2a).

To establish the placental barrier on chip (Fig. 2b), HPVECs were seeded on the embryonic side of the membrane, pre-coated with collagen IV and fibronectin, by flipping the chip upside down. On DIV1, CTBs were seeded on the maternal side, pre-coated with collagen IV, and the chip was inverted to a hanging drop configuration to allow cell sedimentation. After 24 h, a second CTB seeding was performed, necessary to fill the voids originating from the fusion of the first cell batch. At DIV3, dynamic flow was initiated through continuous tilting by ±5°. Daily medium exchange was performed on maternal and embryonic sides.

In parallel to establishing the placental model, hiPSCs were seeded as a single-cell suspension on a hanging drop plate (Fig. 2b) and allowed to sediment at the air-liquid interface for 24 h to form undifferentiated EBs. On DIV1, hiPSCs medium was replaced with EB medium to initiate EB differentiation, and on DIV3, EBs were transferred to a spheroid plate for imaging and continued culturing.

At DIV4 (Fig. 2b), placenta-EB co-culturing was initiated by transferring EBs into the hanging drop beneath the placental barrier. For exposure experiments, compounds were added to the maternal fluidic compartment. On DIV9, the platform was disassembled, and the membrane containing the placental barrier and EB were recovered for downstream analysis (Fig 2c).

The placental barrier was processed for immunofluorescence or electron microscopy to assess morphology and marker expression, while its endocrine and barrier function were assessed by hCG ELISA and compound/NP transport studies. EBs were transferred to a spheroid plate for morphological assessment and germ layer marker analysis by 3D immunostaining. Viability was measured by intracellular ATP at DIV9.

Establishing a placental barrier model on chip

To establish a physiologically relevant placental barrier on chip, primary CTB cells were isolated from human term placenta to form the syncytiotrophoblast layer in the maternal compartment.

The purity of the isolated CTB population was assessed by flow cytometry, showing an average of 93 ±4 % positive cells for the trophoblast marker cytokeratin-7 (CK7) (Supplementary Fig. 2a-d). Morphological assessment of the placental barrier was performed on DIV4, when confluent cell layers of syncytiotrophoblast and endothelium were established on both sides of the membrane, which was confirmed by immunostaining for tubulin (TUB) and VE-cadherin (VE-cad) showing continuous cell layers (Figure 3a-c). The trophoblast layer displayed extensive CK7-positive areas with only few residual mesenchymal cells (e.g. vimentin-positive fibroblasts), confirming high purity of isolated CTBs (Supplementary Fig. 2e, f). Fibroblasts, when present, were typically located beneath the trophoblast layer in direct contact with the membrane, without interrupting the syncytialized layer. Polarization of the trophoblast layer was confirmed by the presence of dense microvilli (Fig. 3d) and the localization of glucose transporter 1 (GLUT1) on the apical surface (Supplementary Fig. 3a). Different densities, shapes, and arrangements of microvilli were observed across regions of the trophoblast layer (Supplementary Fig. 3b, c). TEM micrographs of the trophoblast layer (Fig. 3e and Supplementary Fig. 3d) revealed characteristic features[24] of syncytialized cells, including multinucleation, small mitochondria and apical microvilli.[25–27] Apoptotic bodies and shedding cells, indicative of physiological trophoblast turnover,[24] were also visible. The thin endothelial layer on the embryonic side of the membrane evidenced successful formation of the foetal endothelium (Fig. 3e). To confirm spontaneous syncytialization of the trophoblast layer, the apical fusion marker syndecan-1 (SDC-1) was visualized, indicating formation of a continuous syncytialized layer on the maternal side of the placental barrier (Fig. 3f, g). From DIV4 onward, this layer was referred to as syncytiotrophoblast (STB) layer.

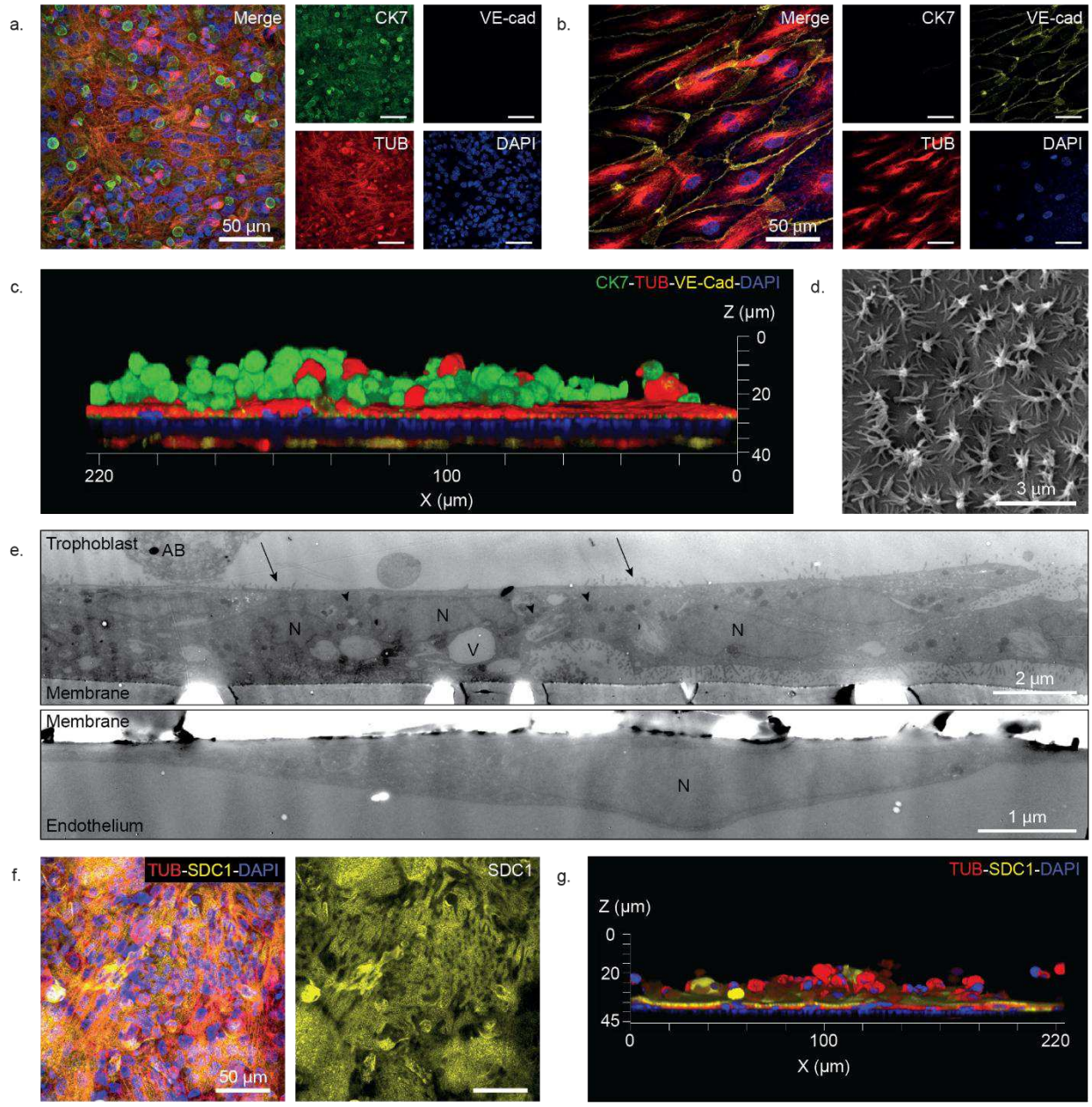

Fig. 3: Morphological assessment of the placental barrier on the chip. a-c, Immunofluorescent staining of trophoblast cells on **a,** the maternal side of the membrane **b,** endothelial cells (HPVECs) on the embryonic side (b) and **c,** 3D rendering orthogonal view of both layers on DIV4. Staining for trophoblast marker (CK7, green), microtubules (tubulin, red), endothelial marker (VE-cadherin, yellow) and nuclei (DAPI, blue). Scale bars: 50 µm. **d,** SEM micrograph of the apical surface of the trophoblast layer showing microvilli. Scale bar: 3 µm. **e,** Stitched TEM images of the trophoblast layer (top, scale bar: 2 µm) and endothelial layer (bottom, scale bar: 1 µm). Multinucleated cells (N, nucleus) are visible on the trophoblast layer, with microvilli (arrows) on the apical side and scattered mitochondria (arrow heads). Apoptotic bodies (AB) and large vesicles and vacuoles (V) can be identified. **f-g,** Immunofluorescent staining of trophoblast cells for the syncytialization marker syndecan-1 (yellow), microtubules (tubulin, red) and nuclei (DAPI, blue) revealing a spontaneously syncytialized layer. Scale bar: 50 µm. **g,** 3D orthogonal rendering of the syncytialized trophoblast.

Placental Model Predicts Physiological Compound Transfer

To evaluate barrier integrity, we quantified transport of molecules of different size across the placental barrier, as size-selective permeability is a key feature of the placental interface. Our findings were consistent with this characteristic: sodium fluorescein (NaF, 0.4 kDa) showed reduced transfer to the embryonic compartment compared to the acellular membrane (Fig. 4a), whereas FITC-dextran (40 kDa) was fully retained, with almost no signal detectable on the embryonic side in the presence of the placental barrier (Fig. 4b).

Moreover, size-dependent translocation was observed for 25 nm and 150 nm poly-methyl-methacrylate (PMMA) NPs, with substantial amounts of 25 nm particles crossing the barrier, while 150 nm particles could not be detected on the embryonic side after 24 h of exposure (Fig. 4c, d). Interestingly, immunofluorescence imaging revealed accumulation of 150 nm PMMA particles on the apical surface of the trophoblast layer, with some particles internalized into the cytoplasm near the nucleus (Fig. 4e).

Compounds with known placental transfer rates from human ex vivo placenta perfusion studies were selected, enabling direct benchmarking of the on-chip barrier. Permeability across the placental barrier and acellular membrane were calculated at 1 h. Among the analysed compounds, antipyrine showed the highest permeability, followed by creatinine, caffeine, acetaminophen, ketoprofen and digoxin (Fig. 4f). Importantly, on-chip transport data strongly correlated with human ex vivo placenta perfusion data (Pearson $r^2 = 0.7374$; Spearman $r = 0.9$), demonstrating that the model captures physiologically relevant placental transport behaviour (Supplementary Fig. 4).

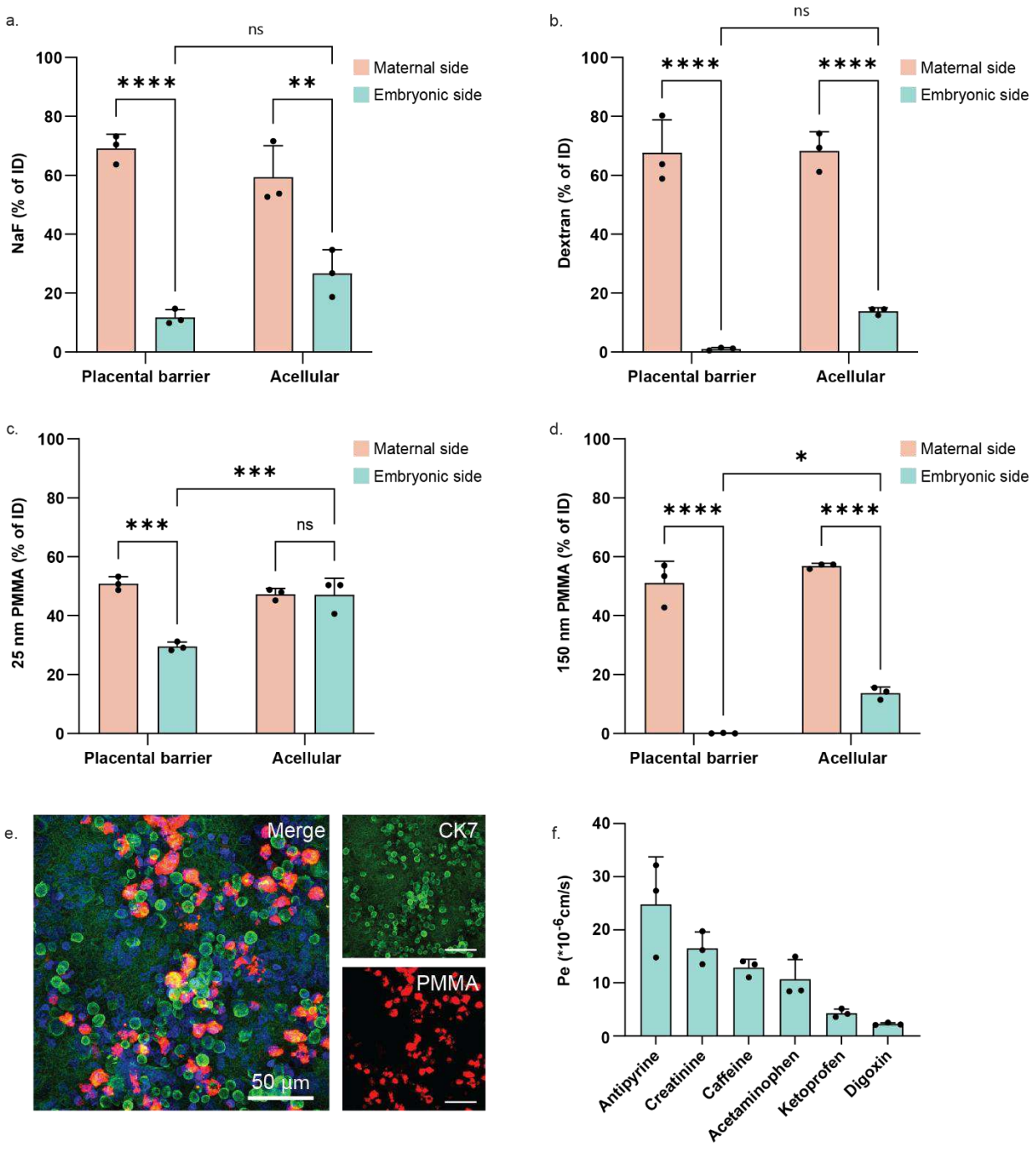

Fig. 4: Placental barrier permeability and transport on chip. a-b, Barrier formation and integrity were assessed at DIV4 using exclusion assays with Na-F (5 µM, 3 h) and 40 kDa FITC-dextran (200 µg/mL, 3 h) in presence (placental barrier) and absence (acellular) of the placental barrier. Data represent mean and SD of n=3 biological replicates, each measured in two technical replicates. Two-way ANOVA with Tukey's post hoc test for multiple comparison; ns= non-significant, ** p≤ 0.01, **** p≤ 0.0001. **c-d,** Transport of 25 nm (500 µg/mL, 24h) and 150 nm (50 µg/mL, 24 h) PMMA NPs from maternal to embryonic compartment in presence (placental barrier) and absence (acellular) of the placental barrier. Data represent mean and SD of n=3 biologically independent experiments, each measured in two

technical replicates. Two-way ANOVA with Tukey's post hoc test for multiple comparison; ns= non-significant; * p≤0.05, *** p≤ 0.001, **** p≤ 0.0001. **e,** Immunofluorescent staining of placental barrier (trophoblast layer) after 150 nm PMMA particles exposure. Staining for trophoblast marker (CK7, green), PMMA particles (Nile red, red), and nuclei (DAPI, blue). Scale bars: 50 µm. **f,** Apparent permeability coefficients (Pe, measured at 1 h) across the placental barrier for 6 compounds: antipyrine, creatinine, caffeine, acetaminophen, ketoprofen, digoxin. Data represent mean and SD of n=3 biologically independent experiments, each measured in two technical replicates.

Integrating EB on chip for Placental-Embryonic Crosstalk

At DIV4, the placental-embryonic interaction was established. After five days of co-culture (DIV9), the placental barrier was assessed for morphological integrity and confluence (Fig. 5a, b). The STB layer displayed aligned, unidirectional microtubules, indicating stable syncytial fusion. Placental barrier integrity was confirmed by reduced Na-F (Fig. 5c) and FITC-dextran (40 kDa, Fig. 5d) permeability compared to the acellular control, although morphological assessment revealed minimal gaps in the STB layer at DIV9, the final experimental day. Syncytialization and endocrine function were further validated by increasing secretion of physiologically relevant concentrations[28] of human chorionic gonadotropin (hCG) from DIV4 to DIV8, with only a slight decrease at DIV9, confirming an active syncytial layer (Fig 5e, f).

EBs co-cultured with the placental barrier under dynamic conditions showed a slightly increased size compared to the ones in the plate and developed a more compact, dense structure (Fig. 5g). Over nine days, EBs differentiated spontaneously into cells of all three germ layers, evidenced by expression of endoderm (GATA6), ectoderm (PAX6, TUBB3), and mesoderm (brachyury) markers (Supplementary Fig. 5). Ectodermal markers appeared earlier and more abundantly, demonstrated by well-developed neural rosettes (PAX6) and βIII-tubulin structures (TUBB3) at DIV9 (Fig. 5h). Neural rosettes were mainly localized in the EB core and partially overlapped with SOX2, consistent with early neuroectodermal identity and the onset of neuronal differentiation.

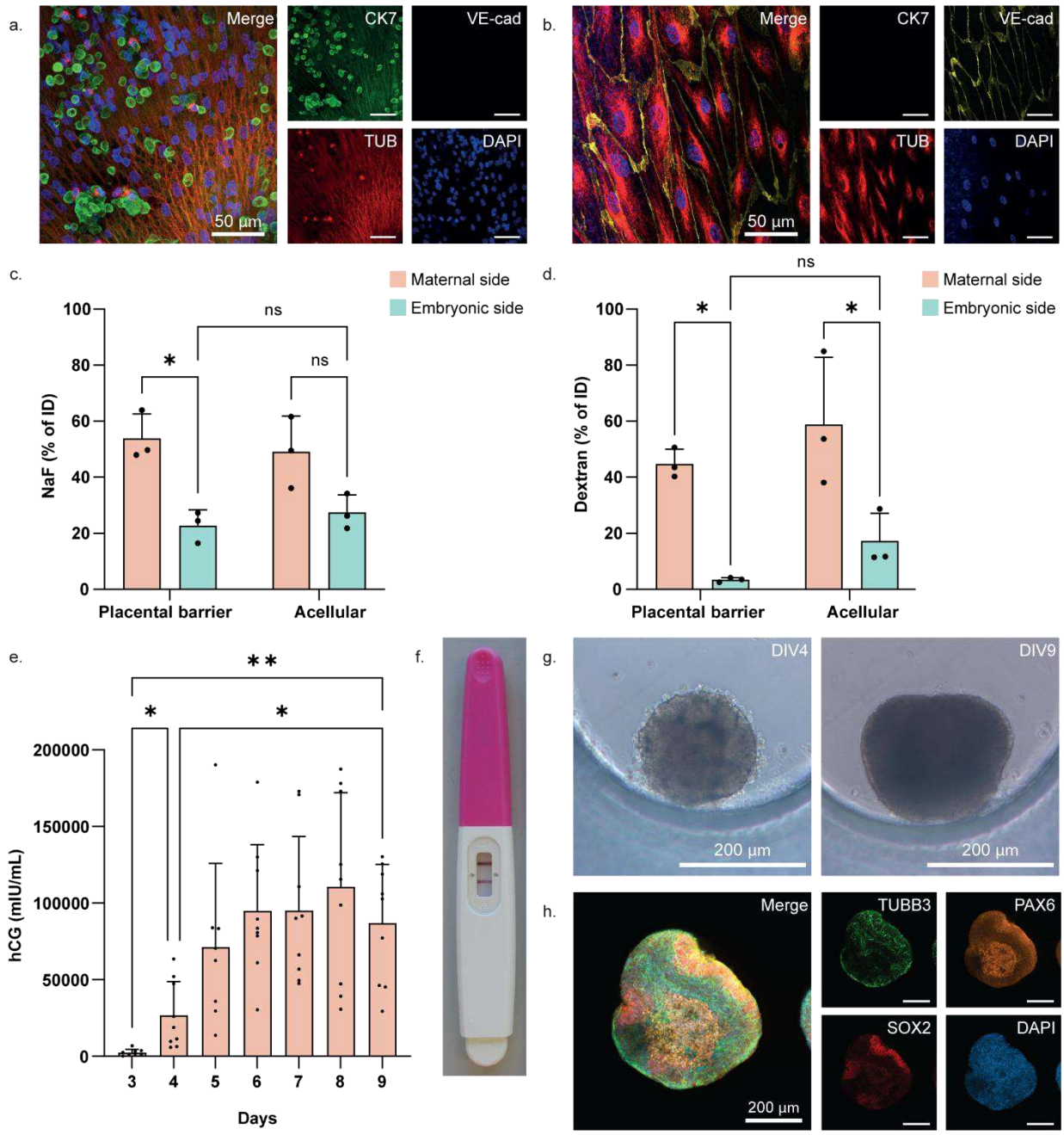

Fig. 5: Prolonged placental barrier culture and EB co-culture model (DIV4-DIV9). a-b, Immunofluorescent staining of **a,** trophoblast cells on the maternal side of the membrane and **b,** endothelial cells on the embryonic side of the membrane at DIV9. Staining for trophoblast marker (CK7, green), microtubules (tubulin, red), endothelial marker (VE-cadherin, yellow) and nuclei (DAPI, blue). Scale bars: 50 µm. **c,** Exclusion assays for Na-F (5 µM, 3 h) and **d,** 40 kDa FITC-dextran (200 µg/ml, 3 h) in presence (placental barrier) and absence (acellular) of the placental barrier. Data represent mean and SD of n=3 independent biological experiments, each measured in at least two technical replicates. Two-way ANOVA with Tukey's post hoc test for multiple comparison; ns = non-significant; * p≤0.05. **e,** Human chorionic gonadotropin (hCG) secretion on chip from DIV3 to DIV9. Data represent mean and SD of n=8-9 independent biological experiments, each measured in two technical replicates. Each dot represents one experiment, the average between 2 units of the same donor. Two-way mixed effects ANOVA with Greenhouse-

Geisser correction and Tukey's post hoc multiple comparison test; * p≤0.05, ** p≤ 0.01. **f,** Pregnancy test on chip with supernatant from DIV6 cultures. **g,** Light microscopy images of EBs before (DIV4) and after (DIV9) co-culture with the placental barrier on chip. Scale bars: 200 µm. **h,** Immunofluorescent staining of EB in co-culture with the placental barrier showing neural rosettes formation. Staining for ectodermal markers βIII tubulin (TUBB3, green) and PAX6 (orange), pluripotency marker SOX2 (red) and nuclei (DAPI, blue). Scale bars: 200 µm.

Microfluidic Placenta Model Demonstrates Active VPA Transport and RA Metabolism

To evaluate the response of the microfluidic co-culture to compound exposure, we perfused the maternal side of the chip with valproic acid (VPA) and all-trans retinoic acid (RA), teratogenic compounds with known developmental neurotoxic effects (Fig. 6a).

To assess the direct effects of VPA on EBs and establish a sub-cytotoxic, developmentally relevant dose for the on-chip experiment, EBs cultured in the well plate were exposed to increasing VPA concentrations (Supplementary Fig. 6). For VPA, morphological alterations were observed at 700 µM, while cytotoxicity was seen at 3000 µM. Therefore, 1000 µM was selected as the concentration for on-chip exposure to achieve exposure levels near the clinically relevant Cmax.[9,13] No major morphological changes were observed in the placental barrier on either side of the membrane at DIV9 upon exposure every 24 h for 5 days to 1000 µM VPA (Supplementary Fig. 7a, b). Trophoblast cells maintained a syncytialized layer after repeated exposure, as evidenced by the expression of the fusion marker SDC-1 (Supplementary Fig. 7c, d). No significant differences of hCG secretion in control and VPA-treated placental barriers were observed, with a progressive increase of hCG levels and only a slight decrease on the last 2 experimental days, confirming the onset of syncytialization (Fig. 6b). Transport of VPA from the maternal to the embryonic side was assessed after 1 h across the placental barrier and acellular membrane (Fig. 6c), revealing an increased concentration on the embryonic side in the presence of the placental barrier compared to the acellular control. At 24 h, equilibrium was reached in the acellular membrane, while enrichment in the embryonic compartment was observed in the presence of the placental barrier, indicating an active transport of VPA.

Previous studies on 2D neural rosette model, have shown that RA concentrations as low as 5 nM are sufficient to disrupt neurodevelopmental processes after direct exposure.[29] To induce measurable developmental perturbations while remaining below cytotoxic levels,[13] we selected 11 nM as a biologically relevant exposure concentration. No significant differences on hCG secretion were observed between RA-treated and untreated placental barriers on DIV9 after five days of repeated exposure (Fig. 6d). 4-hydroxy retinoic acid (4-OH-RA), an important primary metabolite of RA that is less developmentally toxic than the parent compound,[30] was detected on the embryonic side of the chip only in the presence of the placenta indicating active placental

metabolism of RA and suggesting a protective role of the placenta against RA accumulation (Fig. 6e).

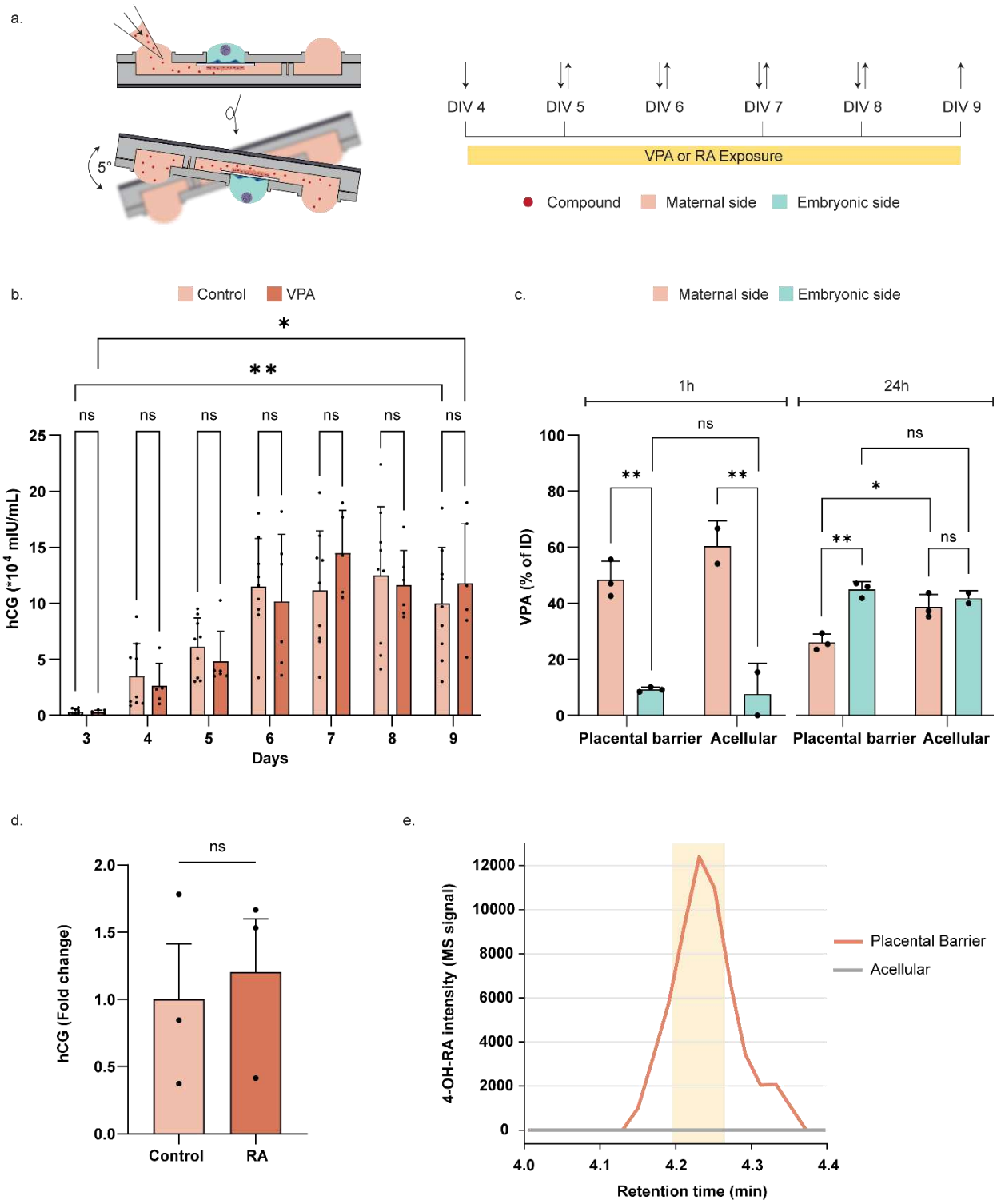

Fig. 6: VPA and RA exposure of the placental barrier on chip. **a,** Schematic of VPA (1000 µM) and RA (11 nM) exposure on chip and experimental timeline from DIV4 to DIV9, with daily exposures. Arrows represent repeated

exposures. **b,** Comparison of hCG secretion on chip from DIV3 to DIV9 in untreated (control) or VPA exposed (VPA) cultures. Data represent mean values and SDs of n=9 (control) and n=5-6 (VPA) independent biological experiments, each measured in two technical replicates. Each dot represents one experiment, the average between 2 units of the same donor. Two-way mixed effects ANOVA with Greenhouse-Geisser correction and Tukey's post hoc multiple comparison test; ns = non-significant; * p≤ 0.05, ** p≤ 0.01. **c,** Translocation of VPA on chip after 1 h and 24 h in the presence (placental barrier) or absence (acellular) of the placental barrier. Data is shown as % of ID. Data represent mean and SD of n=3 independent biological experiments for placental barrier and n=2-3 for acellular experiments, each measured in two technical replicates. Two-way ANOVA with Tukey's post hoc test for multiple comparison; ns= non-significant, * p≤0.05, *p≤0.01, ** p≤ 0.001. **d,** Comparison of hCG secretion on chip on DIV9 in untreated (control) or RA-exposed (RA) cultures. Data represent mean values and SEM of n=3 independent biological experiments, each measured in two technical replicates. Each dot represents one experiment, the average between 2 units of the same donor. X-fold change relative to the untreated control. Statistical analysis: t-test with Welch's corrections; ns = non-significant. **e,** High resolution LC-MS chromatogram of [M+H]+ adduct, based on theoretical mass of 4-hydroxy retinoic acid with 0.001 m/z threshold. Samples were taken from the embryonic compartment, with samples in absence (grey line) or presence (orange line) of the placental barrier in the system.

Placental Regulation of VPA and RA Drives Different Neurodevelopmental Outcomes in EBs

To investigate VPA- and RA-induced embryotoxicity and the contribution of the placental barrier to this effect, EBs were cultured in the microfluidic device either in the absence (monoculture) or presence (co-culture) of the placental barrier to mimic direct and barrier-mediated exposure (Figure 7a and Supplementary Fig. 8).

On DIV9, EBs (control and compound-treated) were stained for ectodermal markers. Control EBs in both monoculture (Fig. 7b and Supplementary Fig. 9a-d; 11a) and co-culture (Fig. 7c and Supplementary Fig. 10a, b; 11b) displayed well-developed ectodermal features, including compact, round neural rosettes (PAX6) and expression of early neuronal markers (TUBB3 and SOX2). Upon VPA exposure, EBs in monoculture (Fig. 7d and Supplementary Fig. 9e-h) showed limited neural rosette elongation, whereas EBs co-cultured with the placental barrier (Fig. 7e and Supplementary Fig. 10c-h) exhibited markedly altered rosette structures, characterized by disrupted morphology and elongated lumens. In contrast, after RA exposure, neural rosette formation of EBs in monoculture was reduced or absent (Fig. 7f and Supplementary Fig. 11c), whereas RA-exposed EBs in co-culture showed neural rosette formation and marker expression, with structures comparable to those of untreated controls (Fig. 7g and Supplementary Fig. 11d). Similarly, VPA exposure in monoculture had limited effects on the presence of the early neuronal marker βIII-tubulin, as control and VPA-exposed EBs showed a dense filament network (Fig. 7h and Supplementary Fig. 9i). In contrast, RA-treated EBs exhibited reduced or delayed early neuronal organization (Fig. 7h and Supplementary Fig. 11e). In co-culture, however, VPA treatment resulted in a pronounced disruption of βIII-tubulin-mediated filament organization, whereas this effect was less evident in monoculture (Fig. 7i and Supplementary Fig. 10i). RA

treatment in co-culture resulted in a less pronounced disruption of early neuronal development, as indicated by βIII-tubulin-positive filament network (Fig. 7i and Supplementary Fig. 11f). After VPA (Fig. 7j) or RA (Fig. 7k) exposure, EBs in both mono- or co-culture remained viable until DIV9, exhibiting slightly elevated ATP levels compared to their untreated controls, which is indicative of preserved metabolic activity. A modest reduction of ATP levels was found in the RA-treated co-cultures.

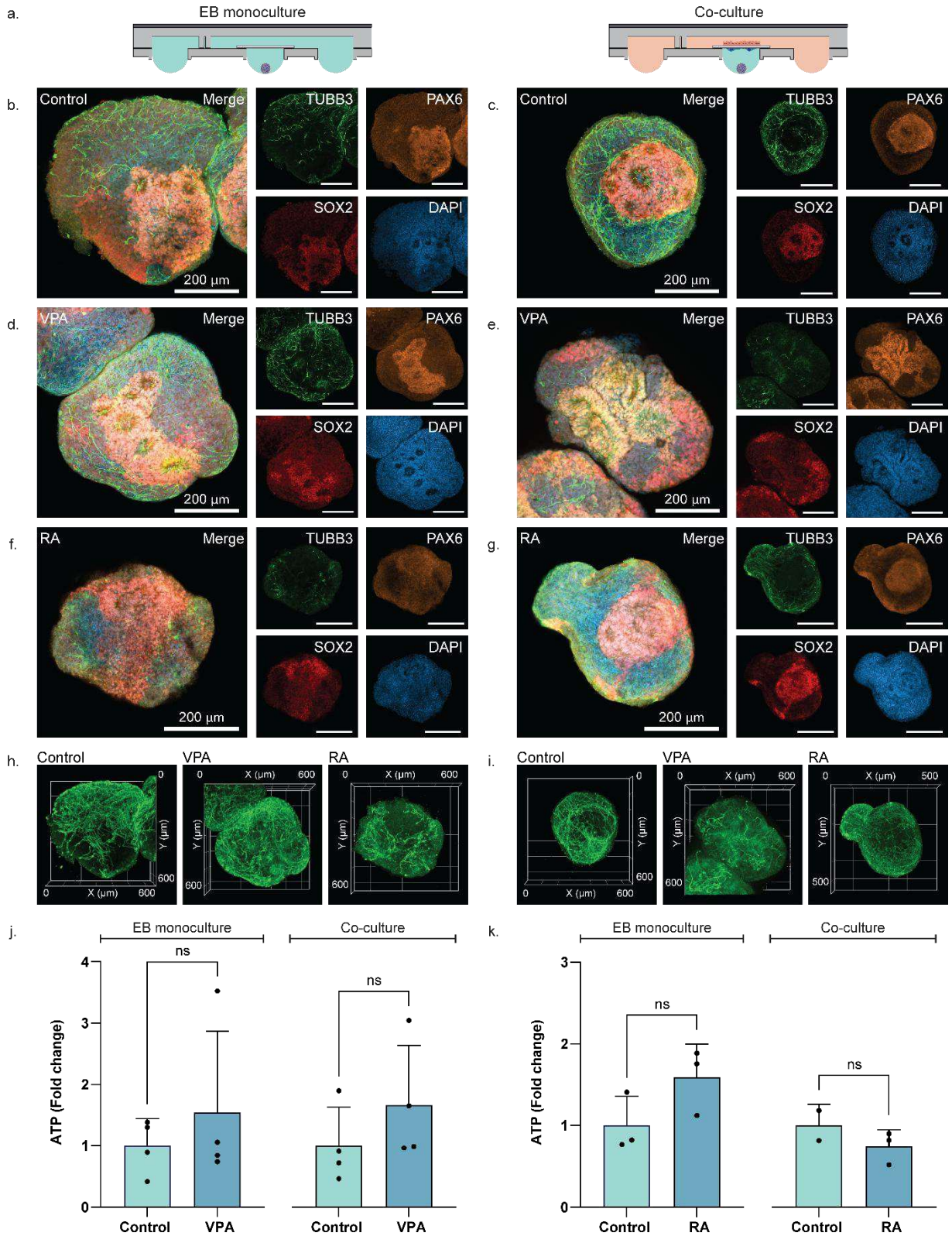

Fig. 7: VPA and RA exposure of EBs on chip in the presence or absence of the placental barrier. a, Schematic of EB culturing on chip for VPA and RA exposure in absence (EB monoculture) or presence (co-culture) of the placental

barrier. **b-e,** Immunofluorescence staining of **b,** EB monoculture control, **c,** EB co-culture control, **d,** EB monoculture exposed to VPA, **e,** EB co-culture exposed to VPA **f,** EB monoculture exposed to RA, **g,** EB co-culture exposed to RA at DIV9. Staining for ectodermal markers βIII tubulin (TUBB3, green) and PAX6 (orange), pluripotency marker SOX2 (red) and nuclei (DAPI). Scale bars: 200 µm. **h-i,** 3D rendering of the early neuronal marker TUBB3 in **h,** EB monoculture control (left), VPA exposed (centre panel), RA exposed (right) and **i,** EB co-culture control (left), VPA exposed (centre), RA exposed (right). **j-k,** ATP release of **j,** EB in monoculture and co-culture at DIV9 in untreated and VPA exposed EBs, and **k,** EB in monoculture and co-culture at DIV9 in untreated and RA exposed EBs shown as fold change to untreated control. Data represent mean values and SDs of n=4 (VPA; n=2 EBs/experiment) and n=3 (RA) independent biological experiments. Statistical analysis of the untreated control: t-test with Welch's corrections; ns = non-significant.

DISCUSSION

In this paper, we present the development of a human-based placenta-embryo microfluidic model that replicates the maternal-embryonic interface, enabling integrated studies of placental transport, functionality, and early embryonic development. The unique device design recreates the cellular architecture of the placental barrier, featuring distinct maternal and embryonic compartments and includes a hiPSCs-derived 3D model of early embryonic development in close vicinity to the barrier, which enables continuous inter-tissue communication. This configuration provides an unprecedented opportunity to assess both, direct effects of substances that translocate to the embryonic compartment and indirect effects caused by placental perturbation of signalling pathways that are critical for embryo-foetal development.[31]

The placental barrier features a syncytialized, polarized trophoblast epithelium[24] with a broad transporter repertoire, which is absent in conventional cell line models that lack spontaneous syncytialization and physiological transporter expression and activity.[32–37] Such limitations can result in altered transport pathways and non-physiological transfer rates. To more faithfully recapitulate placental barrier function, we employed primary cytotrophoblast (CTB) cells from human term placenta, which are non-proliferative but spontaneously fuse into syncytiotrophoblast, a process called syncytialization. However, this fusion process can compromise monolayer continuity, resulting in incomplete barrier coverage. To overcome this challenge, we implemented an optimized double-seeding strategy in which CTB cells were seeded twice on consecutive days (DIV1 and DIV2), ensuring the formation of a confluent syncytiotrophoblast layer on the microfluidic chip. A previous study employed a triple-seeding protocol (days 1, 3, and 7) with EGF supplementation for static insert cultures. [17] In contrast, we adapted and streamlined this concept for a dynamic microphysiological environment, reducing it

to a double-seeding procedure combined with HPVEC co-culturing. Efficient syncytialization was achieved without EGF, thereby avoiding potential activation of non-physiological signalling pathways. Compared to an earlier static CTB monolayer insert culture, which reported STB integrity for 5 days,[38] our placental model culturing was prolonged until DIV9 under dynamic conditions and in the presence of an embryo model. The extended duration and stability enabled the implementation of both acute and repeated exposure scenarios. hCG secretion levels were comparable to those reported in pregnant women, which provided evidence for the physiological relevance of the trophoblast endocrine function. Variability between donors was observed, reflecting physiological differences seen in vivo, where hCG levels are patient- and gestational stage-dependent, peaking around weeks 9–10 at approximately 288,000 mIU/ml.[28]

In vivo data on human placental transfer are scarce due to ethical and technical constraints, leaving a critical gap in understanding transplacental transport during pregnancy. Consequently, ex vivo perfusion of human placenta has become the gold standard for studying transplacental transfer, as it provides physiologically relevant transfer rates that correlate well with clinical observations.[39] Transport rates of drugs and size-dependent NP transfer measured in our microfluidic model closely aligned with data from the ex vivo perfusion system,[40–45] highlighting the translational relevance of our platform. Unlike ex vivo perfusion, which is constrained by limited perfusion duration, low throughput, and a relatively high failure rate, our placenta-embryo chip overcomes these limitations while additionally enabling mechanistic investigation of embryo-foetal effects of translocated substances. All these features highlight the potential of microfluidic placenta models to complement and augment current gold-standard approaches.

To facilitate the assessment of embryo-foetal effects, we incorporated a previously established hiPSCs-derived EB model[13] as a surrogate for early human embryonic development. This model undergoes spontaneous differentiation into the three germ layers, enabling evaluation of early developmental pathways in a 3D context. At DIV9, ectodermal markers and associated morphological features were most prominent, providing a window for qualitative detection of developmental perturbations. In contrast, mesodermal and endodermal lineages were less developed at this early stage, limiting comprehensive analysis of all germ layers within the microfluidic system. Performing EB culturing outside the chip (e.g., off-chip in multiwell plates) and combining it with gene expression analysis could allow for more robust characterization of lineage-specific responses and developmental trajectories in future studies.

A key finding of our study is that exposure to the known teratogen VPA disrupted neuroectodermal differentiation in EBs only when EBs were co-cultured with the placental barrier, revealing a critical role of the placental transfer in modulating embryonic toxicity. This

effect was accompanied by higher VPA concentrations on the embryonic side after 24 h (Fig 6g), providing a plausible explanation for the pronounced abnormalities observed. This interpretation aligns with clinical reports showing higher VPA levels in embryonic compared to maternal circulation.[46,47] VPA is well documented to cause neurodevelopmental abnormalities in the foetus including neural tube defects and other major congenital malformations.[48] In vitro, teratogenic effects have been reported in 2D neural rosette models, where VPA induces lumen disruption, loss of polarity and impaired neurodevelopment marked by TUBB3 dysregulation.[49,50] Here, we extend these findings to a 3D, placenta-coupled system, demonstrating disrupted morphogenesis at 1000 µM maternal VPA occurred only in the presence of the placental barrier, underscoring the importance of the maternal-foetal interface in modulating embryonic exposure and toxicity.

To support our findings with further evidence, we assessed how the placental barrier modulates embryonic responses to RA exposure, as a disruption of neuroectodermal features was only observed in the absence of the placental barrier. RA is an essential developmental morphogen,[51] while excessive or dysregulated RA signalling represents a well-established teratogenic mechanism disrupting embryonic patterning, which underlies craniofacial, cardiac and central-nervous-system malformations.[9,52,53] In vivo, the extent of RA-induced developmental toxicity is influenced by the maternal, placental and embryonic RA metabolisms. Maternal RA reaching the placenta can either be transferred to the foetus or metabolized within the placenta by RA-metabolising enzymes, including CYP26 family members, regulating foetal-embryonic exposure by limiting the availability of bioactive RA.[54] Consistent with this physiological role, the preservation of neural rosette morphology and marker expression in the co-culture model suggests that the placental barrier modulated the effective RA exposure of the EBs, thereby preserving early neuroectodermal organization. In contrast, direct RA exposure in a monoculture resulted in impairment or absence of neural rosette formation, consistent with reports demonstrating that excessive RA disrupts neuroectodermal morphology.[50] Together these findings indicate that our model is capable of recapitulating important physiological functions of the placental barrier and highlight the value of incorporating placental transport and metabolic function into human in vitro developmental toxicity models.

While our platform was demonstrated to yield qualitative, human-relevant data, quantitative assessment will be critical to resolve dose-dependent effects and fully characterise toxicity thresholds with precision. Advanced approaches, such as gene expression profiling or RNA sequencing, could capture subtle or sub-toxic transcriptional changes in EBs, providing mechanistic insights beyond morphological observations.[14] In addition, artificial intelligence and

machine learning-based approaches for quantifying neural rosette formation and morphogenesis or perturbation of specific features of EBs have already been developed[55,56] and could be integrated to enable high-throughput, quantitative analysis. Incorporating these quantitative tools would further enhance the predictive power of the platform.

Overall, this work highlights the importance of integrated, human-relevant in vitro models that capture inter-tissue communication to advance developmental toxicity. By coupling placental transport with embryonic responses in a single system, our platform enables investigation of exposure-response relationships that cannot be obtained using isolated tissue models. This level of biological integration is essential for identifying placenta-mediated effects on embryonic development and represents a critical step toward mechanism-informed, predictive investigation of human developmental toxicity.

METHODS

Sample collection, primary CTB isolation

Term placentae (n=29) were obtained from uncomplicated/healthy pregnancies following caesarean section from the Cantonal Hospital (HOCH) and the Hirslanden Clinic Stephanshorn in St. Gallen, Switzerland. The study was performed under the approval of the local ethics committee (EKOS 20/103; PB_2020-01387) and according to the Declaration of Helsinki, thereby written informed consent was obtained from the pregnant women prior to organ collection.

Primary cytotrophoblast (CTB) cells were isolated adapting the protocol from Petroff et. al.[57] Briefly, approximately 40 g of villous tissue was rinsed in Dulbecco's Phosphate-Buffered Saline (DPBS, Sigma Aldrich) and minced carefully removing large blood vessels. Enzyme digestion was performed in 3 steps, 20 minutes each at 37°C on a horizontal shaker, using a digestion buffer containing 10X trypsin (Thermo Fisher Scientific, 15090046) and 300 U/ml DNase I (Sigma Aldrich, DN25-1G). After every digestion step, supernatant was collected, filtered on a 60-mesh cell dissociation sieve (Sigma Aldrich, CD-1), layered on top of a 1.5 ml foetal bovine serum (FBS; Sigma Aldrich, F9665) and centrifuged at 1000g for 15 min. The cell pellet was resuspended in Dulbecco's Modified Eagle's Medium high glucose (Sigma-Aldrich, D5796) supplemented with 10% FBS and 1% penicillin/streptomycin (P/S, Sigma Aldrich). The obtained cell suspension was filtered using a 100 µm nylon cell strainer (BD Falcon), centrifuged at 1000g for 10 min. After the first centrifugation, the supernatant was collected avoiding the cell pellet and centrifuged again at 1000 g for 10 min. The obtained cell pellets were resuspended in pre-warmed CMF-Hank's containing 10% of 10X HBSS and 2.5% of 1 M HEPES (Sigma Aldrich). The cell suspension was

layered onto two prepared Percoll® gradients (Sigma-Aldrich, P4937) ranging from 70% to 5%, in 50 ml tubes. The gradients were centrifuged at 1200 g for 20 min at room temperature (RT) without a break (Eppendorf centrifuge, 5804 R). After centrifugation, the upper diffuse band was aspirated, and cells between the 30 ml and 15 ml tube mark were collected and washed in culture medium, counted and frozen for further use.

The purity of isolated CTBs (n=22) was determined using flow cytometry (Attune NxT Flow Cytometer, Thermo Fisher Scientific, USA). The cell suspension was fixed and permeabilized in 4% paraformaldehyde (PFA; ROTI®Histofix, Carl Roth, P087.5) and 0.2% Triton X-100 (Sigma-Aldrich) for 10 min at room temperature (RT). Cells were blocked in 5% normal goat serum (NGS; Sigma Aldrich, G6767) in PBS for 45 min at RT. After blocking, cells were stained with CK7 (DAKO, M701829-2) 1:200 or mouse IgG1 kappa 1:1000 (Sigma Aldrich, M9269) in 0.5% bovine serum albumin (BSA; Sigma-Aldrich) in PBS for 45 min at RT. After washing in PBS, Alexa Fluor 488 goat anti-mouse IgG (Invitrogen, A11029) 1:400 in 0.5% BSA in PBS was used as secondary antibody. Analysis was performed using FCS Express 7 (De Novo Software). Cells were first gated based on forward and side scatter properties (FSC-A/SSC-A) to exclude debris. CK7 staining was then used to identify CTB cells and quantify their relative abundance, including isotype and secondary antibody controls to account for nonspecific staining.

Immunofluorescence staining for CK7 (DAKO, M701829-2), epithelial marker specific for trophoblast cells, and vimentin (Abcam, ab92547), characteristic of mesenchymal cells, were performed to identify contaminating fibroblasts in the isolated population.

Cell culture

Human Placental Vascular Endothelial cells (HPVECs) were purchased from ScienCell™ (ScienCell™ Research Laboratories, 7100, USA) and cultured until passage 7, after which a reduced proliferation was observed. Cells were cultivated in fibronectin (ScienCell™ Research Laboratories, 8248) coated T-75 flasks (2 µg/cm^2 in PBS) and passaged upon reaching 80% confluence using 0.25% trypsin-EDTA solution (Sigma-Aldrich). HPVECs were maintained in Endothelial Cell Medium (ECM) supplemented with 5% FBS, 1% Endothelial Cell Growth Supplement and 1% P/S solution (ScienCell™ Research Laboratories, 1001, USA).

A human episomal induced pluripotent stem cell (iPSC) clone was purchased from Gibco™ (A18945, Thermo Fisher Scientific, Waltham, USA). The cell line is a viral-integration-free human iPSC line, generated from cord blood-derived CD34+ progenitors with seven episomal expressed factors (OCT4, SOX2, KLF4, MYC, NANOG, LIN28, and SV40T). The cell line showed no abnormal karyotype alterations up to at least nine passages and has the potential to differentiate into the

3 germ layers.[13,58,59] hiPSCs were used for embryoid body (EB) formation on passage 8, adopting the protocol reported by Jaklin et al.[13]. Briefly, cells were cultivated in Geltrex™ (Thermo Fisher Scientific, A1569601) coated vessels using complete StemFlex™ Medium (Thermo Fisher Scientific, A3349401), supplemented with 10% StemFlex™ Supplement (Thermo Fisher Scientific, A3349401) and, only in case of thawing or passaging, with 1% RevitaCell™ (Thermo Fisher Scientific, A2644501). Cells were passaged at 80% confluence using StemPro Accutase™ Cell Dissociation Reagent (Thermo Fisher Scientific, A1110501) and incubated for 4 min at 37 °C and 5% CO_2. Complete StemFlex™ was added to stop cell detachment, and the cell suspension was centrifuged at 200 g for 4 min. The cell pellet was resuspended in complete StemFlex™, and 24 h after seeding, medium was replaced with StemFlex™ without RevitaCell™.

All cells were maintained in a humidified incubator at 37 °C and 5% CO_2 and passed regular mycoplasma test, with the MycoAlert® Mycoplasma Detection Kit (LT07-418, Lonza, Switzerland).

Microfluidic chip fabrication

A semipermeable PET membrane with a 1 µm pore size, 11 µm thickness and $7*10^{-6}$ pore density (it4ip, Louvain-la-Neuve, Belgium) was laser cut (CO_2 laser, Universal Laser System, Vienna, Austria) into 5x5 mm^2 squares. The membranes were coated with 50 µg/mL human placental collagen IV (Sigma-Aldrich, C5533) for 1 h at 37 °C and 5% CO_2 as previously reported:[21] 50 µl of collagen solution were pipetted on the culture dish to form a drop on which the membrane was placed; another 50 µL drop was then carefully placed on top of the membrane. Following incubation, the membranes were washed in PBS and stored at 4 °C until further use.

The maternal and embryonic layers of the microfluidic chip were designed using Fusion 360 software (AutoDesk, USA). The layers were fabricated from a 3D printed master mold (ceramic-like Perform material, Protolabs, Feldkirchen, Germany) adapting the protocol previously reported by Boos et al.[23] using standard soft lithography techniques. Briefly, polydimethylsiloxane (PDMS) was mixed in a 10:1 (w/w) ratio with the curing agent (Sylgard 184, Dow Corning Corp., Midland, MI, USA), degassed and poured onto the master mold. Following a second degassing step, the PDMS layer was cured at 80 °C for 2.5 h, peeled off the mold and cut into individual chips. The embryonic hanging-drop structures were punched using a 3 mm biopsy punch. The chip was assembled using uncured PDMS prepared by mixing PDMS and curing agent at a 10:3 (w/w) ratio. The uncured PDMS was spin-coated onto a microscope slide (50 mm x 75 mm) at 2500 rpm for 5 min. The embryonic and maternal parts were then brought into contact with the uncured PDMS on the spin-coated slide, and the PET membranes were placed on the backside of the embryonic hanging-drop structures. Next, the maternal and embryonic parts

were bonded together, sandwiching the membrane between the two layers. The assembled chip was then bonded to a microscope glass slide using the same technique. The constructed device was cured overnight at 40 °C and kept afterwards at 4 °C until further use. To reduce evaporation during prolonged culture, 3D-printed frames fitting around the device were used as lids, with the top sealed using sealing tape (Costar, 6524). Prior to cell seeding, chips and lids were sterilized under UV light for 25 min to enable sterile cell culturing in the microfluidic device.

Plasma coating

The PDMS platform was functionalized with thin plasma polymer films deposited via plasma-enhanced chemical vapor deposition (PECVD). Plasma polymer films are considered advanced coatings for functionalizing biomaterials and biological platforms due to their unique properties.[60] Coating the device with these films provides a highly reproducible surface with significantly reduced adsorption or absorption phenomena.

The deposition process was conducted in a capacitively coupled plasma reactor operating at a radiofrequency (RF) of 12.56 MHz. Initially, a cleaning step was performed using an argon plasma for 2 min (argon flow rate: 20 sccm; pressure: 7 Pa; applied power: 20 W). Following this step, the plasma polymerization of hexamethyldisiloxane (HMDSO, Sigma Aldrich, 205389) was carried out.[61] The deposition parameters included a flow rate of 2 sccm HMDSO and 20 sccm Ar, at a pressure of 7 Pa for 10 min, using pulsed power (1 Hz, 50% duty cycle) at 30 W. Pulsed power was employed instead of continuous power to prevent powder formation in the plasma and, consequently, dust contamination on the samples[62]. The same procedure was followed to coat the molds used for the fabrication of PDMS chips. The film thickness was determined by profilometry (Bruker Dektak XT, 12.5 µm stylus radius). The SiO:CH plasma coating is characterized by a high degree of cross-linking resulting in nanopores in the ≤1 nm range.[63]

Microfluidic chip loading for placental barrier model

To avoid evaporation during cell culture, a 96-well plate (Corning) was filled with 200 µL/unit of ultrapure water. An adapted chip holder (Microfluidic chip shop, 10000044) was placed on top of the plate and closed with a lid, creating a humidified chamber for chip culture. Prior to cell seeding, PET membranes were coated on the embryonic side with 2 µg/cm^2 fibronectin and incubated for 5 h at 37 °C and 5% CO_2. The fibronectin solution was removed, and 1.5 x 10^4 HPVECs were seeded on top of the PET membrane in each embryonic unit with 12 µL ECM, without filling the diagonally connected pumping drops. The chip was placed in the humidified chamber in a standing-drop configuration (embryonic side facing upwards) to allow for cell

attachment and kept in an incubator (37 °C and 5% CO_2). After 24 h, the medium on the embryonic side was replaced (12 µL of fresh ECM), and the chip was ready for CTB seeding.
CTBs previously isolated from term placentae were thawed in ECM. A cell suspension of 8 x 10^5 cells/unit in 40 µL ECM was loaded on the maternal side (standing drop configuration) until the PET membrane of the culture chamber was fully covered with liquid. The chip was then flipped to the hanging drop configuration to let the cells attach to the membrane. After 24 h, the maternal side was completely filled with medium (50 µL in total), and a second seeding of CTB cells was performed. For this step, a cell suspension of 2.5 x 10^5 cells/unit in 30 µL was loaded to the maternal side, and the chip was again flipped to the hanging drop configuration. On day in vitro (DIV) 3, a medium exchange was performed. On the maternal side, 10 µL of fresh ECM were added to one hanging drop, and 10 µL were removed from the other hanging drop, repeating this process until a total of 50 µL had been exchanged. On the embryonic side, the medium from the hanging drops was removed, and 10 µL of fresh medium were pipetted into each compartment. Another 10 µL were added to the diagonally connected pumping drops to establish a fluidic network on the embryonic side. The microfluidic channel between the two drops was wetted using a needle (Sterican, 30G). The chip was placed onto a tilting device (InSpheroAG, Multi Bio RS-24) and tilted by ± 5° with a motion time of 20 s at 37 °C and 5% CO_2. Medium exchange on both sides of the membrane was performed daily until DIV9.

Embryoid body (EB) formation

Prior to cell seeding, the outer positions of a 96-well Akura™ PLUS Hanging Drop Plate of the Akura™ PLUS Hanging Drop System (InSphero, CS-PF24, Switzerland) were filled with ultrapure water to reduce evaporation. To obtain comparable EBs among different experiments, 2x 10^3 cells were seeded in each drop using a multi-pipette with 40 µL of StemFlex™ containing 1% RevitaCell™. Cells were cultivated in a hanging-drop system to favour aggregation and EB formation. To start differentiation, after 24 h of culture, StemFlex™ medium was replaced with Embryoid Body Medium (EBM): Knockout™ DMEM (Thermo Fisher Scientific, 10829018), 20% Knockout Serum Replacement, 1% GlutaMAX™, 1% non-essential amino acids, 0.18% beta-Mercaptoethanol (Gibco™, Thermo Fisher Scientific). EBs were transferred to Akura™ 96 Spheroid Plates of the Akura™ PLUS Hanging Drop System (InSphero, CS-PF24, Switzerland) 72 h after seeding (DIV3). Prior to EB transfer, 15 µL of EBM were added to each well of the Spheroid Plate to allow a gentle deposition of the EB. For EB transfer, the hanging drop plate was positioned on top of the Spheroid Plate and 85 µL of medium were pipetted on top of each EB drop, allowing the drop to fall into the Spheroid Plate. Old medium was replaced resulting in a

total medium volume of 70 µL/well. Medium changes using EBM and imaging were performed daily until DIV9.

Placental barrier-EB co-culture on chip

At DIV4, the ECM on the embryonic side of the chip was replaced with EBM (20 µL), and EBs were transferred from the Spheroid Plate to the embryonic drop, establishing the placental barrier-EB co-culture. EBs were picked up from the Spheroid Plate, allowed to settle at the bottom of the pipette tip, and gently placed onto the embryonic drop. The chip was immediately flipped in the hanging drop position to prevent EBs from sticking to the endothelial layer. ECM on the maternal side and EBM on the embryonic side were exchanged daily until DIV9. At the end of the experiment, the EBs were harvested from the chip and transferred to a PBS-filled Akura Spheroid plate for subsequent analysis.

Immunofluorescence staining (placental barrier and EB)

For immunocytochemistry (ICC) of the placental barrier model, cells were fixed and permeabilized in the microfluidic device in 4% PFA (ROTI®Histofix, Carl Roth, P087.5) and 0.2% Triton X-100 (Sigma-Aldrich) for 10 min at room temperature (RT). Subsequently, each unit was blocked in 5% NGS (Sigma Aldrich, G6767) in PBS for 1 h at RT. Primary antibodies (see Supplementary Table 1 for details and dilutions) were diluted in 0.5% BSA (Sigma-Aldrich) in PBS and applied overnight at 4°C. Samples were washed 3 times in PBS followed by incubation with secondary antibodies (see Supplementary Table 1 for details and dilutions) diluted in 0.5% BSA in PBS for 1 h at RT. Afterwards, each unit was washed 3 times in PBS for 5 min at RT, and 40,6-diamidin-2-phenylindol (DAPI) was included in the second washing step. Following the staining, PBS was removed from each unit, and the chip was disassembled. The membranes were recovered and embedded using Mowiol 4-88 (Sigma-Aldrich) overnight at 37 °C, sandwiched between 2 glass coverslips (24x60 mm Huberlab, 10.2355.46 and round 10 mm VWR, 631-0665), allowing for visualization of both sides of the membrane. Images were acquired using a confocal laser scanning microscope (CLSM 780, Zeiss, Germany). Image processing was carried out using ZEN software (version 3.4; Zeiss, Germany).

For ICC of EBs, samples were fixed in Akura plates in 4% PFA (ROTI®Histofix, Carl Roth, P087.5) for 45 min at RT and subsequently washed 3 times in PBS. Staining buffer was prepared mixing 1% Triton X-100 (Sigma Aldrich), 20% DMSO, 10% Normal Donkey Serum (NDS, Jackson ImmunoResearch Europe), 0.05% Tween 20 (Sigma Aldrich) in PBS. EBs were transferred to an Eppendorf tube with 100 µl staining buffer and incubated for 3 h on a shaker. Primary antibodies

were diluted in staining buffer, and EBs were incubated in the staining solution at 4 °C overnight. After 3 washing steps with PBS for 30 min at RT, secondary antibodies were diluted in staining buffer, and EBs were incubated in the staining solution for 3 h at RT. After the washing steps were performed, EBs were transferred to a 96-well plate (Corning, Costar, 3603) and embedded in a drop of 2% low-gelling agarose (Sigma Aldrich, A9414). To perform tissue clearing, 50 µl/well of FocusClearTM (CellExplorer, FC-101) were added directly on top of the agarose-embedded EBs and incubated for 30 min at RT. Images in FocusClearTM were acquired with ECHO-revolve and Zeiss LSM980 MP. Image processing was carried out using ZEN software (version 3.4; Zeiss, Germany) and ImageJ Software (1.54).

Permeability studies

To assess barrier tightness and integrity, exclusion of sodium fluorescein (Na-F, Sigma-Aldrich) and 40 kDa FITC-dextran (Sigma-Aldrich) were determined at DIV4 and DIV9, representing the first and last day of EB-placenta co-culture experiments, respectively. 50 µL of 5 µM Na-F or 200 µg/mL FITC-dextran in ECM without phenol red (ScienCell, SCI1001-prf) were loaded into the maternal compartment, and 20 µL of ECM without phenol red were added to the embryonic side. Permeability assays were performed on membranes containing the placental barrier as well as acellular controls. After 3 h of incubation under dynamic conditions at 37 °C and 5% CO_2, 7 µL aliquots from the maternal and the embryonic side were collected, transferred into a 96-well plate, diluted in ECM without phenol red, and fluorescent tracer molecules were detected using a microplate reader (BioTek Synergy H1 Multimode Reader) at an excitation wavelength of 485 nm and emission of 528 nm. The amount of each marker on the maternal and embryonic side was corrected for the medium blank and expressed as a percentage of the initial dose (ID) from 3 biological replicates (3 different donors) with 2 technical replicates each.

Characterization and translocation of NPs

Fluorescently labelled polymethylmethacrylate (PMMA) NPs of 2 different sizes were purchased: 25 nm PMMA micromer® greenF particles (Micromod, 29-00-251) and 150 nm Nile Red, fluorescent PMMA (Spherotech, FPMA-0256-2), delivered respectively as 10 µg/mL suspension and 0.2% w/v in water. Stock solutions were vortexed before each use. To characterize the NPs, their hydrodynamic diameter and zeta potential were measured at 500 µg/mL (25 nm PMMA) or 50 µg/mL (150 nm PMMA) in 10% PBS in ultrapure water (Milli-Q) and ECM (Zetasizer Ultra instrument, Malvern Instruments, UK). Measurements of hydrodynamic diameter were repeated after 24 h at 37 °C to mimic NP exposure conditions. Particles were visualized using transmission

electron microscopy (TEM). Briefly, 25 µL NP suspension were incubated for 1 min on a 200-mesh copper grid with continuous carbon film (Electron Microscopy Resolutions, C200Cu100). The carbon grids were pretreated with a 3 min incubation on a 300 µL droplet of 0.1% (w/v) poly-l-lysine solution (PLL, P8920, Sigma-Aldrich) and blotted on Whatman filter paper after PLL and NP suspension incubation. Grids were imaged using a JEOL JEM-2100Plus TEM-STEM microscope at 200 kV with a JEOL SightSKY TEM Camera. Characteristics of the PMMA NPs are summarized in Supplementary Table 2.

To assess placental translocation, NPs were diluted to the above-mentioned concentrations, in phenol red-free ECM, vortexed again for 30 s and immediately loaded into the chip on the maternal side (50 µL). On the embryonic side, each unit and pumping drop were filled with a total of 20 µL ECM without phenol red. After 24 h incubation (37 °C and 5% CO_2) under dynamic condition, 7 µL of samples were collected separately from the maternal and the embryonic side and added to a 96-well plate diluted in ECM without phenol red. Translocation was assessed for membranes containing the placental barrier as well as acellular controls. Fluorescence signal was measured using a microplate reader (BioTek Synergy H1 Multimode Reader) at the respective excitation and emission wavelengths; 474 nm and 525 nm for the 25 nm PMMA, 559 nm and 635 nm for the 150 nm PMMA. NP concentration was determined by trendline application on the blank-corrected sample values of 3 biological replicates with 2 technical replicates each.

Translocation of drugs

To compare drug transport across the placental barrier with ex vivo placental perfusion data, the translocation of the following compounds was assessed on the placental barrier as well as acellular membranes at DIV4: 100 µM antipyrine (Sigma-Aldrich, A5882, CAS 60-80-0), 100 µM and 1000 µM valproic acid (VPA, Sigma-Aldrich, PHR1061, CAS 99-66-1), 100 µM ketoprofen (Sigma Aldrich, K1751, CAS 22071-15-4), 100 µM digoxin (Sigma Aldrich, D6003 CAS 20830-75-5), 100 µM caffeine (Fluka, 27600, CAS 58-08-2), 100 µM acetaminophen (paracetamol, Sigma Aldrich, A7302, CAS 103-90-2) and 0.5 mg/mL creatinine (Sigma Aldrich, C4255, CAS 60-27-5). Ketoprofen, digoxin and caffeine were dissolved in DMSO; antipyrine, acetaminophen and creatinine were dissolved in ultrapure water, VPA was dissolved directly in the ECM. Vehicles and blank controls were also measured. The working solution of each compound was added to the maternal side of each chip unit. After 1 h (and 24 h for VPA), 10 µL samples were collected from the maternal and embryonic sides of each unit.

Transport of antipyrine, VPA, ketoprofen, digoxin, caffeine and acetaminophen were assessed using high performance liquid chromatography coupled to tandem mass spectrometry (HPLC-ESI-

MS/MS). The 10 µL samples were diluted in 90 µL extraction solvent (10% Milli-Q water + 90% LCMS grade methanol) and centrifuged at 4 °C for 5 minutes at 14,000 g prior to HPLC-ESI-MS/MS analysis. The transport of creatinine was assessed using the epoc® Blood Analysis System (Siemens Healthineers). Concentrations below the lower limit of quantification (LLOQ) were set to zero for analysis.

The permeability (P) coefficient, expressed in cm/s, was determined using the formula:

$$\frac{\Delta Q/\Delta t}{A * C0}$$

in which ΔQ is the amount of compound X transported in the embryonic compartment in a time frame Δt (1 h), A is the cell surface area (exchange area), and C_0 is the initial concentration of the assessed compound. Each P coefficient was corrected for the influence of the acellular membrane to obtain the apparent permeability P_e:

$$\frac{1}{\frac{1}{Pm} - \frac{1}{Pc}}$$

where the permeability across the membrane P_m was subtracted from the permeability across the cells P_c.

Relative apparent permeability (P_{app}) ratios were determined by expressing the P_{app} coefficient as a fraction of the P_{app} coefficient obtained for antipyrine with the formula:

$$\frac{\text{Ae, compound X (t)} * \text{Am, antipyrine (t0)}}{\text{Ae, antipyrine (t)} * \text{Am, compound X (t0)}}$$

in which A_e, compound X (t) = amount of compound X in the embryonic compartment at time point t (1 h or 24 h); A_m, antipyrine (t0) = amount of antipyrine added to the maternal compartment at time point t0; A_e, antipyrine (t) = amount of antipyrine in the embryonic compartment at time point t; and A_m, compound X (t0) = amount of compound X added to the maternal compartment at time point t0. The relative P_{app} ratios were used for the correlation with the transport indexes (TIs) reported for the ex vivo placental perfusion model.[40–44]

HPLC-ESI-MS/MS quantification

Quantification used a Vanquish Core HPLC (Thermo Fisher Scientific) coupled to an Orbitrap IDX Tribrid mass spectrometer (Thermo Fisher Scientific). Chromatography was performed with a Synergi 4 µm Polar-RP 80 Å LC column (30 mm x 2 mm) with SecurityGuard guard cartridge (Phenomenex). The flow rate was 0.7 mL/min at a column temperature of 40 °C and mobile phases were LCMS grade water (A) and acetonitrile (B) with 0.1% formic acid. The mobile phase gradient was 5% B from 0 to 0.1 min, brought to 100% B between 0.1 to 1.8 min, kept at 100% B

from 1.8 to 2.35 min, brought to 5% B between 2.35 to 2.4 min, and kept at 5% B from 2.4-2.8 min followed by a 1 min injection sequence. The injection volume was 5 µL. A targeted MS/MS method was used to measure caffeine, antipyrine, ketoprofen, acetaminophen, and digoxin, while a targeted single ion monitoring (tSIM) method was used to measure valproic acid with a resolving power of 120,000 from 133-207 *m/z*. Additional MS data acquisition and processing parameters are reported in Supplementary Table 3. Chemical stocks were prepared at a concentration of 100 mM in DMSO for caffeine, ketoprofen, and digoxin, and Milli-Q water for antipyrine and acetaminophen. Stocks were diluted in ECM, and extracted using the same method as samples (9:1 dilution in 90% methanol) to prepare calibration points at concentrations of 50 nM, 100 nM, 500 nM, 1 µM, 5 µM, 10 µM, and 15 µM. Pure valproic acid is a liquid and was diluted directly in ECM and extracted using the same method as samples to prepare calibration points of 1 µM, 2.5 µM, 5 µM, 10 µM, 25 µM, 100 µM, and 500 µM. Samples were analysed grouped by chemical exposure, and a calibration curve was analysed before and after each group of samples. Peak areas of all monitored transitions (targeted MS/MS) and precursor (tSIM) were integrated, manually checked, and used for quantification and data analysis. Calibration points were used to generate linear models with $1/ X^2$ regression weighting in Skyline software v. 24.1.0.199.[64] R-squared values for all calibration models were greater than 0.95. Calculated concentrations for samples below the lowest point of the calibration curve were considered below the LLOQ.

Electron Microscopy characterization (TEM and SEM)

For transmission and scanning electron microscopy (TEM/SEM) analysis, membranes containing the placental barrier model were recovered at DIV4 from the chip, washed twice in PBS and fixed in 3% glutaraldehyde (Sigma-Aldrich) in 0.1 M sodium cacodylate buffer (Electron Microscopy Sciences, pH 7.4) for 15 minutes at RT as a modification of our previously published protocols.[65] After disassembling the chip, to allow for simultaneous processing of the two sides of the membrane for TEM imaging, each membrane was pinched on a needle and attached to an Eppendorf tube, so that it remained in the center of the tube and always in solution. A second incubation in fixative was performed for 10 minutes at RT, followed by a third incubation in the fixative for 25 minutes at 4 °C. Each sample was washed twice in 0.2 M Na-cacodylate buffer (Electron Microscopy Sciences, pH 7.4) for 20 minutes at 4 °C. Samples were kept at 4 °C in fresh Na-cacodylate buffer until further processing using TEM or SEM.

For TEM, the membranes on needles were then stained with 2% osmium tetroxide (OsO_4, Electron Microscopy Sciences) in 0.1 M Na-cacodylate buffer for 2 hours at 4 °C and washed once

for 7 minutes at RT and once for 3 minutes at 4 °C in Milli-Q water. Subsequently, the samples were dehydrated through a graded ethanol series at 4 °C (10 min 50%, 10 min 75%, 2 × 15 min 100% EtOH from HoneyWell, Riedel-de-Haen, then 3× 30 min 100% water-free EtOH from Sigma-Aldrich). Afterwards, an incubation in 100% acetone (Sigma Aldrich) at RT, followed by an Epon gradient in acetone (33% Epon at 4 °C overnight, 66% at 4 °C for 6 h, 100% at RT for 2 h with the tube lid open for acetone evaporation) using Epon 812 substitute resin (Epoxy embedding kit 45359, Sigma-Aldrich, Germany) were performed. Membranes were finally embedded in 100% Epon resin inside molds and cured at 60 °C for 48 hours. Ultrathin sections (80 to 100 nm in thickness) were prepared using an ultramicrotome (Leica EM UC6, Germany), placed on Formvar-coated copper grids (100 mesh, EM Resolutions), air-dried, and imaged at different magnifications at 80 kV with a Zeiss EM 900 microscope (Carl Zeiss Microscopy GmbH, Germany). To better visualize the two cell layers on both membrane sides, sequentially acquired TEM images of both layers along the membrane were stitched together using an ImageJ stitching plug-in.[66]
To assess the polarization of the trophoblast layer, we analysed the microvilli presence on its surface using SEM. The samples were processed as for TEM, yet after fixation the membranes were dehydrated with an Ethanol (HoneyWell, Riedel-de-Haen) series (30 min 50%, 30 min 70%, 30 min 80%, 60 min 90% and 60 min 100% Ethanol) at RT, followed by an incubation with hexamethyldisiloxane (HMDSO, 205389, Sigma-Aldrich) for 30 min at RT. After overnight drying at RT, membranes were glued onto SEM stubs with the trophoblast layer facing upwards, sputter-coated with 10 nm carbon and subsequently gold-palladium in a high vacuum coater (Leica EM ACE 600), and imaged using an Axia ChemiSEM (Thermo Fisher Scientific) microscope at 10 kV with 65 pA and an ETD detector.

hCG ELISA

Human chorionic gonadotropin (hCG) ELISA was performed for untreated (control) samples and VPA-treated samples from DIV3 to DIV9 and RA-treated samples on DIV9. As previously described[3], 96-well high binding assay plates (Corning, 9018) were pre-coated at 4 °C overnight with the capture antibody rabbit anti-hCG (Dako, A0231) diluted 1:1000 in a 50 mM $NaHCO_3$ buffer. Wells were washed using a 0.1% Tween-20/PBS and blocked (1% BSA/PBS) for 1.5 h at RT. Samples with appropriate dilutions (DIV3 1:200; DIV4 1:2000; DIV5 to DIV9 1:6000; RA DIV9 1:8000) were prepared. A serial dilution of hCG standard (BioSupply UK, HOR-250) was prepared from a stock solution (1 µg/mL in 1% BSA/PBS) with concentrations ranging from 6000 pg/mL as the highest concentration, followed by 4000, 2000, 1000, 500, 250, 125, and 0 pg/mL. Following washing (0.1% Tween20/PBS), 100 µl of standard and samples were placed in the respective wells

and incubated in a humidified chamber for 1 h at 37 °C. After washing, 100 µl of the detection antibody mouse anti-hCG (Serotec, MCA 1436; 1:5000 in 1% BSA/PBS) were pipetted into the desired wells and incubated 1 h at 37 °C in a humidified chamber. After washing, the secondary detection antibody was added (goat anti-mouse IgG HRP, Biorad, 1706516, 1:5000 in 1% BSA/PBS) and incubated in a humidified chamber at 37 °C for 1 h. After the last washing step, 100 µL of 3,3',5,5'-Tetramethylbenzidine (TMB) were pipetted into the wells. Plates were incubated for 15 min at RT, protected from light. Optical density (OD) was measured at 650 nm (SynergyH1, BioTek). The OD signal from each sample and standard was corrected for the medium blank and expressed as a mIU/mL. Experiments with 8 different donors for the controls and 6 different donors for the VPA treatment were analysed with 2 technical replicates for each condition.

Viability assay

The ATP content of EBs was evaluated by using the CellTiter-Glo® 3D Cell Viability Assay (Promega) following the manufacturer's instructions. Briefly, samples were washed twice with PBS, then 20 µL of PBS and 20 µL of reagent were added to each sample, blank and standard, pipetting up and down to mechanically disrupt the EBs. All samples were transferred to a Half Area LUMITRAC™ plate (Greiner Bio-One, 675075). EBs obtained from the microfluidic chip were diluted 1:10 in PBS to fit into the standard curve. The luminescence signal was measured after 30 min with a microplate reader (BioTek Synergy H1 Multimode Reader). The signal was corrected for the PBS blank, normalised to the respective control and expressed as fold change to the untreated control from 4 biological replicates with 2 technical replicates each (n=2 EBs/experiment/condition) for VPA samples and n=3 biological replicates for RA.

Valproic acid compound treatment

As proof of concept, VPA (Sigma-Aldrich, PHR1061) was used as a known neuro-teratogenic compound. On DIV4 the placental barrier-EB co-culture and EB monoculture on-chip were exposed to 1000 µM VPA. Working solutions for VPA were prepared by dissolving the stock solution in ECM or EBM freshly before exposure and vortex it for 1 min prior to usage to achieve a homogeneous solution. VPA in ECM (placental barrier-EB co-culture) or VPA in EBM (EB monoculture) was added to the maternal compartment (50 µL), and 20 µL EBM were applied to the embryonic compartment. Treatment was repeated every 24 h, exchanging medium on both sides of the membrane until DIV9 under dynamic conditions. To establish a dose-response curve, EBs were treated in Akura™ 96 Spheroid Plates with 0, 4, 12, 37, 111, 333, 700, 800, 1000, 3000 µM VPA, with 3000 µM previously described as a cytotoxic concentration.[13] Briefly, VPA was

dissolved in EBM as described above. EBs were cultivated in 70 µL EBM until DIV9. From DIV4, the medium was removed every 24 h and replaced with the respective VPA concentration. Morphological changes were monitored daily, and images were taken using an Axio Imager 2 (Zeiss).

Retinoic acid compound treatment, metabolism, and measurement

As proof of concept, RA (Sigma-Aldrich, R2625) was used as a known teratogen compound. On DIV4, the EB monoculture and placental barrier-EB co-culture on chip were exposed to 11 nM RA. Working solutions for RA were prepared by dissolving the stock solution in DMSO. Working solutions were prepared in EBM or ECM freshly before exposure and vortexed for 30 s prior to usage to achieve a homogeneous solution. RA in ECM (placental barrier-EB co-culture) or RA in EBM (EB monoculture) were added to the maternal compartment (50 µL), and 20 µL EBM were applied to the embryonic compartment. Exposure was repeated every 24 h, with complete medium replacement on both sides of the membrane until DIV9 under dynamic conditions.

To detect the 4-OH-RA metabolite formation, RA was added on DIV4 to the maternal side of the chip as described above in presence or absence (acellular membrane) of the placental barrier. The chip was placed in the incubator (37 °C, 5% CO_2) and operated under dynamic conditions. After 24 h, 10 µL of medium from the embryonic side of each condition was collected, diluted in 90 µL LCMS grade methanol and stored at -20 °C. Subsequently, samples were then centrifuged at 4 °C for 5 minutes at 14,000 g, then 95 µL transferred to a clean microcentrifuge tube, and dried in a rotary evaporator at RT until dry (about 30 minutes). Dried samples were reconstituted in 20 µL of 9:1 methanol/ water (v/v) including 100 nM sulfamethoxazole as an internal standard, and the entire contents transferred to an amber LC-MS vial with glass microinsert. HPLC-ESI-MS/MS analysis was performed as described above, with the following modifications. The LC flow rate was 0.2 mL/min and the gradient was brought from 5% B to 100% B from 0.1 to 6.5 minutes, held at 100% B until 8.4 minutes, and returned to 5% B by 8.5 minutes and kept at 5% B until 11 minutes. Sample injection volume was 10 µL. A tSIM scan was collected between 300-320 *m/z* in addition to targeted MS/MS scans described in Supplementary Table 3. Representative LC-MS and LC-MS/MS chromatograms were plotted using three-point smoothing for visualization.

Statistical analysis

Statistical significance was assessed using the statistical tests indicated in each figure caption. Experimental sample sizes are also reported in the figure captions. Data were analysed using GraphPad Prism (GraphPad Prism version 10.5, GraphPad Software, La Jolla California USA,

http://www.graphpad.com). Immunofluorescent staining on placenta and EB was performed at least n=3, and a representative image is shown in the main figures.

DATA AVAILABILITY

All data supporting the findings of this study are available within the Article and Supplementary Information. Source data supporting the findings of this study are openly available in Zenodo at https://doi.org/10.5281/zenodo.18478217, reference number 18478217. Drug transport raw data have been deposited to MetaboLights[67] repository with the study identifier MTBLS13922. The raw image data sets and reconstructed-image data are available from the authors for research purposes on reasonable request.

ACKNOWLEDGMENTS

This research received financial support from the Stiftung ProCare Schweiz, the European Union (EU) through the UPRISE Project (European Health and Digital Executive Agency (HADEA), under the HORIZON-HLTH-2024-ENVHLTH program (grant agreement number – 101156622), the Swiss National Science Foundation through the NCCR “Antiresist” (Contract number 51NF40_180541, J.A.B, A.H.), and the Swiss State Secretariat for Education, Research and Innovation (SERI, contract no. 25.00057). The authors acknowledge the use of AI tools to improve grammar and flow of the manuscript. We acknowledge the Single Cell Facility of the Department of Biosystems Science and Engineering of the ETH Zurich for their support. We thank Dr. Davide Bottone for assistance with the processing of the TEM and SEM images. We also acknowledge the obstetric, midwifery and clinical research staff at the participating hospitals for their essential support with participant recruitment and sample collection. We sincerely thank the pregnant women who generously and voluntarily donated placental tissue for this study.

AUTHOR CONTRIBUTIONS

M.M., J.A.B., and T.B.-T. conceived and designed the study; M.M. fabricated the microfluidic devices, performed all the on- and off-chip experiments, analysed, interpreted and visualized data, wrote the manuscript with additional input from all co-authors; I.W initially established the EB culture protocol; X.L. established the 3D imaging protocol; V.K. processed and imaged the TEM and SEM samples; J.F. performed the HPLC-MS analysis; P.N. established and performed the plasma coating; J.B. designed the microfluidic chip and performed EB imaging; J.A.B. and T.B.-T. supervised the study; T.B.-T. and A.H. acquired funding. All authors edited and approved the final manuscript.

COMPETING INTERESTS

No conflict of interest to declare.

REFERENCES

1. Buerki-Thurnherr, T., Schaepper, K., Aengenheister, L. & Wick, P. Developmental Toxicity of Nanomaterials: Need for a Better Understanding of Indirect Effects. *Chem. Res. Toxicol.* **31**, 641–642 (2018).
2. Bové, H. *et al.* Ambient black carbon particles reach the fetal side of human placenta. *Nature Communications 2019 10:1* **10**, 3866- (2019).
3. Dugershaw-Kurzer, B. *et al.* Nanoparticles Dysregulate the Human Placental Secretome with Consequences on Angiogenesis and Vascularization. *Adv. Sci. (Weinh).* **11**, (2024).
4. Mitchell, A. A. *et al.* Medication use during pregnancy, with particular focus on prescription drugs: 1976-2008. *Am. J. Obstet. Gynecol.* **205**, 51.e1-51.e8 (2011).
5. Lupattelli, A. *et al.* Medication use in pregnancy: a cross-sectional, multinational web-based study. *BMJ Open* **4**, 4365 (2014).
6. Haas, D. M. *et al.* Prescription and Other Medication Use in Pregnancy HHS Public Access. *Obstet Gynecol* **131**, 789–798 (2018).
7. Mansour, O. *et al.* Prescription medication use during pregnancy in the United States from 2011 to 2020: trends and safety evidence. *Am. J. Obstet. Gynecol.* **231**, 250.e1-250.e16 (2024).
8. Zafeiri, A., Mitchell, R. T., Hay, D. C. & Fowler, P. A. Over-the-counter analgesics during pregnancy: a comprehensive review of global prevalence and offspring safety. *Hum. Reprod. Update* **27**, 67–95 (2021).
9. Agency, E. M. Committee for Medicinal Products for Human Use ICH S5 (R3) guideline on reproductive toxicology: Detection of Toxicity to Reproduction for Human Pharmaceuticals Step 5. www.ema.europa.eu/contact (2020).
10. Seiler, A. E. M. & Spielmann, H. The validated embryonic stem cell test to predict embryotoxicity in vitro. *Nat. Protoc.* **6**, 961–978 (2011).
11. Genschow, E. *et al.* The ECVAM international validation study on in vitro embryotoxicity tests: Results of the definitive phase and evaluation of prediction models. *Alternatives to Laboratory Animals* **30**, 151–176 (2002).
12. Powles-Glover, N. *et al.* New approach methodologies for assessing developmental toxicity of pharmaceuticals: Case examples and future directions. *Reproductive Toxicology* **137**, 109035 (2025).
13. Jaklin, M. *et al.* Focus on germ-layer markers: A human stem cell-based model for in vitro teratogenicity testing. *Reproductive Toxicology* **98**, 286–298 (2020).
14. Jaklin, M. *et al.* Optimization of the TeraTox Assay for Preclinical Teratogenicity Assessment. *Toxicological Sciences* **188**, 17–33 (2022).
15. Aye, I. L. M. H., Tong, S., Charnock-Jones, D. S. & Smith, G. C. S. The human placenta and its role in reproductive outcomes revisited. *Physiol. Rev.* (2025).
16. Baergen, R. N., Burton, G. J. & Kaplan, C. G. Benirschke's Pathology of the Human Placenta: Seventh Edition. *Benirschke's Pathology of the Human Placenta: Seventh Edition* 1–939 (2021).
17. Hemmings, D. G., Lowen, B., Sherburne, R., Sawicki, G. & Guilbert, L. J. Villous Trophoblasts Cultured on Semi-permeable Membranes form an Effective Barrier to the Passage of High and Low Molecular Weight Particles. *Placenta* **22**, 70–79 (2001).
18. Fuenzalida, B. *et al.* Modelling the maternal-fetal interface: An in vitro approach to investigate nutrient and drug transport across the human placenta. *J. Cell. Mol. Med.* **28**, (2024).

19. Blundell, C. *et al.* A microphysiological model of the human placental barrier. *Lab Chip* **16**, 3065 (2016).
20. Miura, S., Sato, K., Kato-Negishi, M., Teshima, T. & Takeuchi, S. Fluid shear triggers microvilli formation via mechanosensitive activation of TRPV6. *Nat. Commun.* **6**, 1–11 (2015).
21. Aengenheister, L. *et al.* An advanced human in vitro co-culture model for translocation studies across the placental barrier. *Sci. Rep.* **8**, 1–12 (2018).
22. Gonçalves, I. M. *et al.* Placental microphysiological systems: new advances on promising platforms that mimic the microenvironment of the human placenta. *Lab Chip* **25**, 979–995 (2025).
23. Boos, J. A. *et al.* Microfluidic Co-Culture Platform to Recapitulate the Maternal–Placental–Embryonic Axis. *Adv. Biol.* **5**, 1–12 (2021).
24. Jones, C. J. P. & Fox, H. Ultrastructure of the normal human placenta. *Electron Microsc. Rev.* **4**, 129–178 (1991).
25. Acharya, S. *et al.* Exploring placental ultrastructure: A review of electron microscopy techniques and emerging methods for resolving 3D organelle architecture. *Placenta* **54**, 323–329 (2026).
26. Martinez, F., Kiriakidou, M. & Strauss, J. F. Structural and Functional Changes in Mitochondria Associated with Trophoblast Differentiation: Methods to Isolate Enriched Preparations of Syncytiotrophoblast Mitochondria. *Endocrinology* **138**, 2172–2183 (1997).
27. Tozawa, S. *et al.* Upregulation of Autophagy During the Differentiation of Primary Human Term Cytotrophoblast Cells into Syncytial Cells: Ultrastructural Analysis. *International Journal of Molecular Sciences 2025, Vol. 26, Page 1321* **26**, 1321 (2025).
28. Korevaar, T. I. M. *et al.* Reference ranges and determinants of total hCG levels during pregnancy: the Generation R Study. *European Journal of Epidemiology 2015 30:9* **30**, 1057–1066 (2015).
29. Dreser, N. *et al.* Development of a neural rosette formation assay (RoFA) to identify neurodevelopmental toxicants and to characterize their transcriptome disturbances. *Arch. Toxicol.* **94**, 151–171 (2020).
30. Isoherranen, N. & Zhong, G. Biochemical and physiological importance of the CYP26 retinoic acid hydroxylases. *Pharmacol. Ther.* **204**, 107400 (2019).
31. Buerki-Thurnherr, T., Schaepper, K., Aengenheister, L. & Wick, P. Developmental Toxicity of Nanomaterials: Need for a Better Understanding of Indirect Effects. *Chem. Res. Toxicol.* **31**, 641–642 (2018).
32. Jokimaa, V. *et al.* Expression of syndecan-1 in human placenta and decidua. *Placenta* **19**, 157–163 (1998).
33. Hori, T. *et al.* Trophoblast stem cell-based organoid models of the human placental barrier. *Nature Communications 2024 15:1* **15**, 1–15 (2024).
34. Illsley, N. P. CURRENT TOPIC: Glucose Transporters in the Human Placenta. *Placenta* **21**, 14–22 (2000).
35. Evseenko, D. A., Paxton, J. W. & Keelan, J. A. ABC drug transporter expression and functional activity in trophoblast-like cell lines and differentiating primary trophoblast. *Am. J. Physiol. Regul. Integr. Comp. Physiol.* **290**, (2006).
36. Vachalova, V. *et al.* Functional reorganization of monoamine transport systems during villous trophoblast differentiation: evidence of distinct differences between primary human trophoblasts and BeWo cells. *Reproductive Biology and Endocrinology 2022 20:1* **20**, 112- (2022).
37. Sadovsky, Y. & Jansson, T. Comparative expression patterns of selected membrane transporters in differentiated BeWo and human primary trophoblast cells. *Placenta* **72–73**, 48–52 (2018).
38. Huang, X. *et al.* Establishment of a confluent monolayer model with human primary trophoblast cells: Novel insights into placental glucose transport. *Mol. Hum. Reprod.* **22**, 442–456 (2016).

39. Hutson, J. R., Garcia-Bournissen, F., Davis, A. & Koren, G. The human placental perfusion model: A systematic review and development of a model to predict in vivo transfer of therapeutic drugs. *Clin. Pharmacol. Ther.* **90**, 67–76 (2011).
40. Li, H., Van Ravenzwaay, B., Rietjens, I. M. C. M. & Louisse, J. Assessment of an in vitro transport model using BeWo b30 cells to predict placental transfer of compounds. *Arch. Toxicol.* **87**, 1661–1669 (2013).
41. Poulsen, M. S., Rytting, E., Mose, T. & Knudsen, L. E. Modeling placental transport: Correlation of in vitro BeWo cell permeability and ex vivo human placental perfusion. *Toxicology in Vitro* **23**, 1380–1386 (2009).
42. Conings, S. *et al.* Transplacental transport of paracetamol and its phase II metabolites using the ex vivo placenta perfusion model. *Toxicol. Appl. Pharmacol.* **370**, 14–23 (2019).
43. Mose, T. *et al.* Placental Passage of Benzoic acid, Caffeine, and Glyphosate in an Ex Vivo Human Perfusion System. *J. Toxicol. Environ. Health A* **71**, 984–991 (2008).
44. Lagrange, F., Pehourcq, F., Bannwarth, B., Leng, J. J. & Saux, M. C. Passage of S-(+)- and R-(-)-ketoprofen across the human isolated perfused placenta. *Fundam. Clin. Pharmacol.* **12**, 286–291 (1998).
45. Furer, L. A. *et al.* Novel electrospun chitosan/PEO membranes for more predictive nanoparticle transport studies at biological barriers. *Nanoscale* **14**, 12136–12152 (2022).
46. Brown, L. T. L., Pereira, D. & Winn, L. M. A Narrative Review on the Effect of Valproic Acid on the Placenta. *Birth Defects Res.* **117**, (2025).
47. Sandvik, D. *et al.* In vitro models of valproic acid to assess neurodevelopmental toxicity: A scoping review. *Epilepsia* **66**, 2170–2181 (2025).
48. Ornoy, A. Valproic acid in pregnancy: How much are we endangering the embryo and fetus? *Reproductive Toxicology* **28**, 1–10 (2009).
49. Zhang, X. Z. *et al.* Folic Acid Rescues Valproic Acid-Induced Morphogenesis Inhibition in Neural Rosettes Derived From Human Pluripotent Stem Cells. *Front. Cell. Neurosci.* **16**, 888152 (2022).
50. Dreser, N. *et al.* Development of a neural rosette formation assay (RoFA) to identify neurodevelopmental toxicants and to characterize their transcriptome disturbances. *Arch. Toxicol.* **94**, 151–171 (2020).
51. Cunningham, T. J. & Duester, G. Mechanisms of retinoic acid signalling and its roles in organ and limb development. *Nature Reviews Molecular Cell Biology 2015 16:2* **16**, 110–123 (2015).
52. Samrani, L. M. M. *et al.* Nervous system development related gene expression regulation in the zebrafish embryo after exposure to valproic acid and retinoic acid: A genome wide approach. *Toxicol. Lett.* **384**, 96–104 (2023).
53. Piersma, A. H., Hessel, E. V. & Staal, Y. C. Retinoic acid in developmental toxicology: Teratogen, morphogen and biomarker. *Reproductive Toxicology* **72**, 53–61 (2017).
54. Isoherranen, N. & Zhong, G. Biochemical and physiological importance of the CYP26 retinoic acid hydroxylases. *Pharmacol. Ther.* **204**, 107400 (2019).
55. Lundin, B. F. *et al.* RosetteArray® Platform for Quantitative High-Throughput Screening of Human Neurodevelopmental Risk. *bioRxiv* 2024.04.01.587605 (2024) doi:10.1101/2024.04.01.587605.
56. Shankar, V., Pappa, A. Z., van Blitterswijk, C., Vrij, E. & Giselbrecht, S. Morphometric-Assisted Prediction of Developmental Toxicity Using Stem Cell-Based Embryo Models in Microwells. *Adv. Healthc. Mater.* **14**, 2404847 (2025).
57. Petroff, M. G., Phillips, T. A., Ka, H., Pace, J. L. & Hunt, J. S. Isolation and culture of term human trophoblast cells. *Methods Mol. Med.* **121**, 203–217 (2006).
58. Burridge, P. W. *et al.* A Universal System for Highly Efficient Cardiac Differentiation of Human Induced Pluripotent Stem Cells That Eliminates Interline Variability. *PLoS One* **6**, e18293 (2011).

59. Yu, J. *et al.* Induced pluripotent stem cell lines derived from human somatic cells. *Science (1979).* **318**, 1917–1920 (2007).
60. Coad, B. R., Favia, P., Vasilev, K. & Griesser, H. J. Plasma polymerization for biomedical applications: A review. *Plasma Processes and Polymers* **19**, 2200121 (2022).
61. Hegemann, D. *et al.* Plasma polymerization of hexamethyldisiloxane: Revisited. *Plasma Processes and Polymers* **18**, 2000176 (2021).
62. Watanabe, Y., Shiratani, M., Kubo, Y., Ogawa, I. & Ogi, S. Effects of low-frequency modulation on rf discharge chemical vapor deposition. *Appl. Phys. Lett.* **53**, 1263–1265 (1988).
63. Franke, J. *et al.* Consideration of the effect of nanoscale porosity on mass transport phenomena in PECVD coatings. *J. Phys. D Appl. Phys.* **57**, 405303 (2024).
64. Adams, K. J. *et al.* Skyline for Small Molecules: A Unifying Software Package for Quantitative Metabolomics. *J. Proteome Res.* **19**, 1447–1458 (2020).
65. Gupta, G. *et al.* Boron Nitride Nanomaterials Trigger Immunomodulatory Effects in Human Broncho-Epithelial Cells by Modulating Eicosanoid Lipid Signaling. *Advanced Science* (2025).
66. Preibisch, S., Saalfeld, S. & Tomancak, P. Globally optimal stitching of tiled 3D microscopic image acquisitions. *Bioinformatics* **25**, 1463–1465 (2009).
67. Yurekten, O. *et al.* MetaboLights: open data repository for metabolomics. *Nucleic Acids Res.* **52**, D640–D646 (2024).

Supplementary Files

This is a list of supplementary files associated with this preprint. Click to download.

- NatureCommreportingsummaryMM.pdf
- 2026MurdeuetalSupplementaryinformationunlinked.docx